Cardioprotective factors against myocardial infarction selected in vivo from an AAV secretome library

Giulia Ruozi[1]†, Francesca Bortolotti[1,2]†, Antonio Mura[1], Mateusz Tomczyk[1,3], Antonella Falcione[1], Valentina Martinelli[1], Simone Vodret[4], Luca Braga[1,3], Matteo Dal Ferro[2], Antonio Cannatà[2,3], Lorena Zentilin[1], Gianfranco Sinagra[2,5], Serena Zacchigna[4,5], Mauro Giacca[1,3,5]*

Therapies for patients with myocardial infarction and heart failure are urgently needed, in light of the breadth of these conditions and lack of curative treatments. To systematically identify previously unidentified cardioactive biologicals in an unbiased manner in vivo, we developed cardiac FunSel, a method for the systematic, functional selection of effective factors using a library of 1198 barcoded adeno-associated virus (AAV) vectors encoding for the mouse secretome. By pooled vector injection into the heart, this library was screened to functionally select for factors that confer cardioprotection against myocardial infarction. After two rounds of iterative selection in mice, cardiac FunSel identified three proteins [chordin-like 1 (Chrdl1), family with sequence similarity 3 member C (Fam3c), and Fam3b] that preserve cardiomyocyte viability, sustain cardiac function, and prevent pathological remodeling. In particular, Chrdl1 exerted its protective activity by binding and inhibiting extracellular bone morphogenetic protein 4 (BMP4), which resulted in protection against cardiomyocyte death and induction of autophagy in cardiomyocytes after myocardial infarction. Chrdl1 also inhibited fibrosis and maladaptive cardiac remodeling by binding transforming growth factor–β (TGF-β) and preventing cardiac fibroblast differentiation into myofibroblasts. Production of secreted and circulating Chrdl1, Fam3c, and Fam3b from the liver also protected the heart from myocardial infarction, thus supporting the use of the three proteins as recombinant factors. Together, these findings disclose a powerful method for the in vivo, unbiased selection of tissue-protective factors and describe potential cardiac therapeutics.

INTRODUCTION

Heart failure (HF) has reached epidemic proportions, affecting ~64 million people and standing as the main cause of death and disability (*1*). Despite the remarkable progress in the clinical management of patients and the use of ventricular assist devices (*2*), the prognosis of HF remains poor, with mortality estimated at 6 to 7% at 1 year (*3*). Thus, there is an urgent need to develop new treatments to prevent HF.

An essential component underlying this epidemic burden of HF is the loss of cardiomyocytes (CMs) in adult life, paralleled by the inability of these cells to undergo renewal. This loss can be marked during myocardial infarction (MI), when as many as 25% of the total 2 to 4 billion cells in the left ventricle (LV) can die (*4*). Therapeutic reperfusion by percutaneous coronary intervention immediately after MI reduces the infarcted area but contributes to CM death itself by sudden oxidative stress (*5*). CM deficiency is not accompanied by relevant new CM generation after birth. The normal adult human heart is estimated to have less than 50% regenerative capacity over a 70-year lifetime (*6*), well below what would be required to compensate for pathological loss.

These considerations indicate that the goal of preventing CM death is of paramount importance. Unfortunately, no drug or treatment is currently effective for this purpose. Over the past years, several studies have shown that brief episodes of coronary occlusion/reperfusion preceding or after MI (ischemic pre- and postconditioning, respectively) can reduce infarct size; even ischemia/reperfusion in distant organs (remote ischemic conditioning) can confer cardioprotection [reviewed in (*7*–*9*)]. Unfortunately, these studies have not yet translated into clinically effective applications (*10*). Most of these investigations have focused on treatments that increase viable myocardium immediately after MI, essentially by measuring protection from sudden lack of oxygenation followed by reoxygenation. This approach, however, fails to provide information on events that occur at later times from ischemia/reperfusion but are equally essential to determine long-term CM survival and cardiac function. These include, among others, the extent of perfusion and collateral flow formation, the efficiency in removal of dysfunctional mitochondria, and the activation of intracellular protective pathways. These events are activated several hours after the acute ischemic events and determine the fate of a vast number of CMs in the so-called area at risk (*11*), which can be as large as 88% of the original infarct region (*12*). Developing a molecule or a therapeutic strategy that protects CMs in these areas of uncertain fate immediately after MI and throughout reperfusion would be of immense therapeutic value.

Here, we sought to identify, in a fully unbiased and systematic manner, the cellular proteins that can exert cardioprotective activity after MI and to rank them according to their individual potency. We report the generation of an arrayed library of 1198 adeno-associated virus (AAV) barcoded vectors that encode for factors from the mouse secretome and a method, which we named cardiac FunSel, for their functional screening in vivo. This functional selection process led to the identification of three previously undescribed proteins (Chrdl1,

[1]Molecular Medicine Laboratory, International Centre for Genetic Engineering and Biotechnology (ICGEB), 34139 Trieste, Italy. [2]Cardiovascular Department, ASUGI, 34149 Trieste, Italy. [3]British Heart Foundation Centre of Research Excellence, School of Cardiovascular Medicine and Sciences, King's College London, London SE5 9NU, UK. [4]Cardiovascular Biology Laboratory, International Centre for Genetic Engineering and Biotechnology (ICGEB), 34139 Trieste, Italy. [5]Department of Medical, Surgical and Health Sciences, University of Trieste, 34149 Trieste, Italy.
*Corresponding author. Email: mauro.giacca@kcl.ac.uk
†These authors contributed equally to this work.

Fam3c, and Fam3b) that exert powerful cardioprotective activity after MI by suppressing CM apoptosis and stimulating protective autophagy. We found that the cardioprotective activity of Chrdl1, an antagonist of bone morphogenetic protein (BMP) during embryonic development (*13*), ensues from both preserving CM viability by blocking the negative effects of BMP4 on CM autophagy and inhibiting cardiac fibrosis and remodeling after MI by suppressing the negative effect of transforming growth factor–β (TGF-β) on cardiac fibroblasts. The identification of Chrdl1 and the other cardioprotective proteins paves the way to the development of novel biological therapeutics for MI.

RESULTS

Systematically selecting cardioprotective factors in mice

Our previous proof-of-principle work in skeletal muscle has shown that in vivo selection from pools of AAV vectors can be used to identify factors protecting against muscle fiber death (*14*). We therefore wanted to (i) adapt the selection process to the systematic, automated screening of a large AAV vector collection; (ii) develop a library corresponding to all secreted factors (the secretome); and (iii) directly screen this AAV library for factors exerting protective activity against acute myocardial ischemia, which could eventually be used as biotherapeutics. To achieve these goals, we developed cardiac FunSel (Fig. 1A). Pools of 50 vectors at a time were generated from an AAV serotype 9 (AAV9) cDNA library. Every pool was injected into the heart at a relatively low multiplicity of infection, by which the complexity of vectors entering each target cell is reduced. Then, MI was induced to stimulate cell selection. Most myocytes died; however, cells expressing protective factors gained selective advantage and survived. After 3 weeks, vector DNA was recovered from the survived myocardium, and the frequency of each vector was determined by next-generation sequencing (NGS), detecting a DNA barcode within the viral genome, which univocally identifies each factor. Barcode read frequencies were compared to those in noninfarcted animals injected with the same AAV9 pool and to those in the viral preparation before injection. When a vector induced CM protection, it was positively selected and, thus, enriched over the others. The opposite holds true for factors favoring CM death. Our previous proof-of-principle evidence using 40 factors had indicated that multiple AAV vectors can be packaged simultaneously, infectivity of vector pools is maintained in vivo, and transgene expression is proportional to vector dilution in the viral mix (*14*, *15*).

Because cardioprotection after MI requires prompt expression of viral transgenes after vector administration, we determined the kinetics of AAV-mediated cardiac transduction after MI. After intramyocardial AAV9 injection, transgene expression was detected as early as 2 hours after MI and was increased about 10 times in the subsequent 4 hours and an additional 10 times after 12 hours (Fig. 1B). Thus, intramyocardial AAV injection after MI results in prompt expression of the delivered vectors and supports the feasibility of FunSel in the heart.

Generation of a mouse secretome library in AAV vectors

To apply cardiac FunSel in a systematic manner, we generated an arrayed library of AAV vectors coding for the mouse secretome. In each vector, the cDNA coding portion of a mouse secreted factor was cloned downstream of the constitutive cytomegalovirus (CMV) immediate early (IE) promoter and a synthetic intron and was followed by a 20–nucleotide (nt) sequence for NGS adapter annealing and a unique 10-nt sequence barcode (Fig. 1C). We started by considering 2033 unique proteins identified in the mouse genome that displayed a signal peptide and lacked a transmembrane domain or intracellular localization signal and were, thus, potentially secreted (*16*). In addition, we also included factors that are released outside the cells through unconventional secretion pathways [such as fibroblast growth factor 2 (FGF2) and interleukin-1 (IL-1) (*17*)]. The relatively small size of the AAV genome, limiting cDNA cloning to 5 kb including the promoter and regulatory regions, reduced the number of cDNAs to 1604 genes (78.9%; fig. S1A). The availability of physical cDNA clones from the Mouse Genome Collection (MGC) (*18*, *19*), IMAGE (*20*), or FANTOM libraries (*21*) further trimmed the number of factors to a final complexity of 1198 individual AAV clones (Fig. 2A and table S1). Abundant and rare transcripts are equally represented in this arrayed collection of clones, which is composed of cytokines, growth factors, hormones, chemokines, interleukins, extracellular matrix proteins, secreted enzymes, and other Gene Ontology (GO) categories of secreted proteins, including a few hundred novel proteins of unknown function (fig. S1B). After cloning and characterization, we organized the vectors into 24 pools of 50 factors each according to insert length to avoid bias in packaging (*14*). Most vectors in all pools had comparable packaging efficiency, as determined by barcode NGS of viral lysates (z score within ±1.96 for 1170 of 1200 vectors, which corresponds to 95% of the distribution; Fig. 2B).

In vivo functional selection of factors protecting the heart after MI

Each 50-vector AAV9 pool was injected into the LV of eight adult CD1 mice immediately after MI and of six mice without infarction. Each heart was injected with 30 μl of a vector pool preparation with a titer of 1×10^{12} viral genomes/ml to minimize transduction of a single cell by multiple vectors (*14*). This also limits the probability of bystander CM coselection, namely, that a CM transduced with an irrelevant vector is coselected with a CM secreting a cardioprotective protein.

After 3 weeks, animals were euthanized, cardiac DNA was extracted, and barcodes were polymerase chain reaction (PCR) amplified and sequenced by NGS. Cumulative barcode recovery for each of the 24 AAV9 pools is shown in fig. S1C. For each of the factors in the 24 vector pools, we determined the ratio between the number of reads in animals with and without MI, along with the confidence intervals of each distribution at 95 and 99% (fig. S2, blue and red dotted line, respectively). This ratio is independent of virus packaging efficiency. Factors with a total number of reads ≥50 were considered in the analyses. Only 24 factors out of the 1198 tested showed reads below this threshold and were not analyzed further; 16 of these were included in pool 23, which contains the vectors with the longest cDNA inserts.

To permit comparison among the 24 different vector pool distributions, z scores were assessed for all vectors' log(MI/sham) ratios (table S2). Overall, the 1% tails of the distributions consisted of 21 factors, of which 15 exerted positive (z score ≥ 2.58) and 6 negative (z score ≤ 2.58) function. Additional 37 vectors were within the 5% tails (15 positive and 22 detrimental; z score ± 1.96). Figure 2C schematically shows the cumulative results obtained from the entire secretome library with the indication of the 1 and 5% confidence intervals. Compared to vector distribution in the original library, the

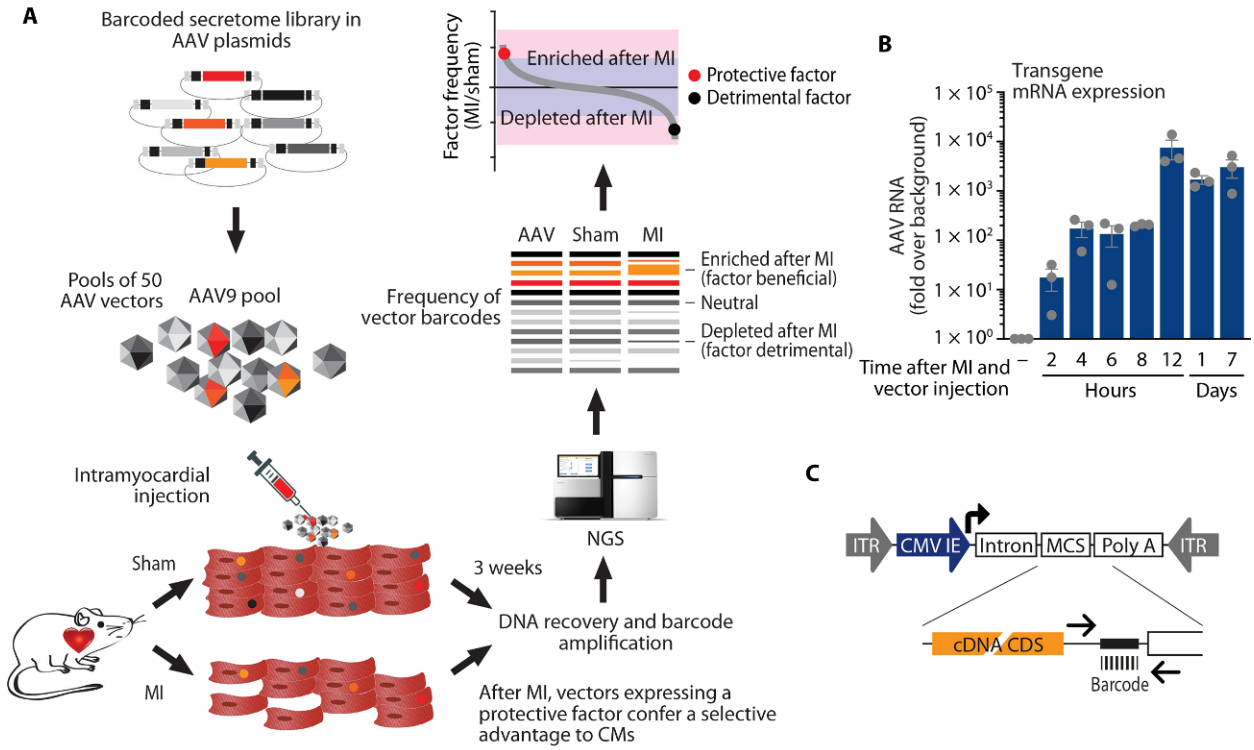

Fig. 1. In vivo functional selection of cardioprotective proteins. (**A**) Schematic illustration of FunSel for cardioprotection. A pool of plasmids coding for different factors is used to generate a pool of AAV9 vectors, which are then injected intramyocardially in mice; each vector transduces different cardiomyocytes (CMs). Selection is then applied by inducing MI. After 3 weeks, barcoded vector DNA is PCR amplified and sequenced by next-generation sequencing (NGS). Factors exerting cardioprotective activity are relatively enriched in CMs. (**B**) Evaluation of the onset of AAV-mediated expression in the infarcted heart. AAV9-ZsGreen vectors were delivered to the infarct border region immediately after MI, and expression was evaluated at the indicated time points after injection. Values show the amount of transgene mRNA upon normalization for endogenous hypoxanthine guanine phosphoribosyltransferase (HPRT) (means ± SEM; $n = 3$ per time point, three samples per animal). (**C**) Schematic representation of the pGi vector plasmid used for the secretome library generation. The primers to amplify the 10–base pair (bp) barcode region are indicated by black arrows. The pGi AAV-backbone plasmid also contains two inverted terminal repeat (ITR) sequences, essential for recombinant AAV vector production. CDS, coding sequence; CMV IE, cytomegalovirus immediate early promoter ; MCS,Multiple cloning site; polyA: polyadenylation site.

GO categories that were statistically enriched after selection were those for growth factor, hormone, calcium, and, in particular, developmental protein (fig. S1B).

Cardiac FunSel is a competitive method that allows ranking efficacy of the selected factors once tested together. Therefore, we obtained four additional AAV9 pools (pools A to D; table S3), each composed of 50 vectors, to establish a final hierarchy of potency. These final 200 vectors included the 58 factors characterized by z score ≥ 1.96 in pools 1 to 24 plus an additional 142 factors from the original 24 pools. These additional factors, which are highlighted in bold black letters in table S2, were selected among the additional top 2 to 10 of each of the 24 pools' distributions.

These 200 selected vectors were assigned to the four 50-vector groups according to insert length to permit comparable packaging efficiency. The four pools were then used for in vivo selection in eight infarcted and six control mice per pool. AAV packaging efficiency and virus barcode recovery for NGS for all vectors in the four pools are shown (fig. S3, A and B, respectively). The ratio between the number of reads in sham animals and animals with MI, along with the confidence intervals of each factor distribution at 95 and 99% (blue and red dotted line respectively), is in fig. S3C. The cumulative results for this second round of screening are summarized in Fig. 2D. Three factors resulted in enrichment with a z score ≥ 2.58 and four factors with a z score ≥ 1.96 (table S3 in red and blue, respectively).

The top seven performers included five proteins for which no information is available relative to cardiac biology. These were two members of the family with sequence similarity 3 (Fam3), Fam3b and Fam3c (*22*, *23*), both from pool B; the NHL repeat-containing protein 3 (Nhlrc3) (*24*) and chordin-like 1 (Chrdl1) (*13*) from pool C; and the HtrA (Htra1) protein (*25*) from pool D. The other two selected proteins were both in pool A and are midkine (Mdk), which was reported to exert a protective role against cardiac injury (*26*), and relaxin-1 (Rln-1), which belongs to the relaxin family of proteins for which there is evidence on cardiovascular effects (*27*, *28*). Selection of these last two factors was considered a good indication of the efficacy of cardiac FunSel.

Analysis of the 100 factors that were negatively selected according to the GO terms revealed an enrichment for inflammatory chemokines and cytokines. At least seven of these negative factors [Mmp7 (*29*, *30*), Fstl3 (*31*, *32*), CCl21 (*33*, *34*), CCl3 (*35*, *36*), Fgf23 (*37*, *38*), Cxcl2 (*39*, *40*), and IL-9 (*41*–*43*)] have already been reported to individually worsen cardiac function after MI (fig. S4). This further strengthens the effectiveness of the selection process. We did not consider the negatively selected factors further in the continuation of this study.

Efficacy of individual cardioprotective factors

The five novel selected factors identified by FunSel plus Mdk as a reference positive control were chosen for further individual investigation.

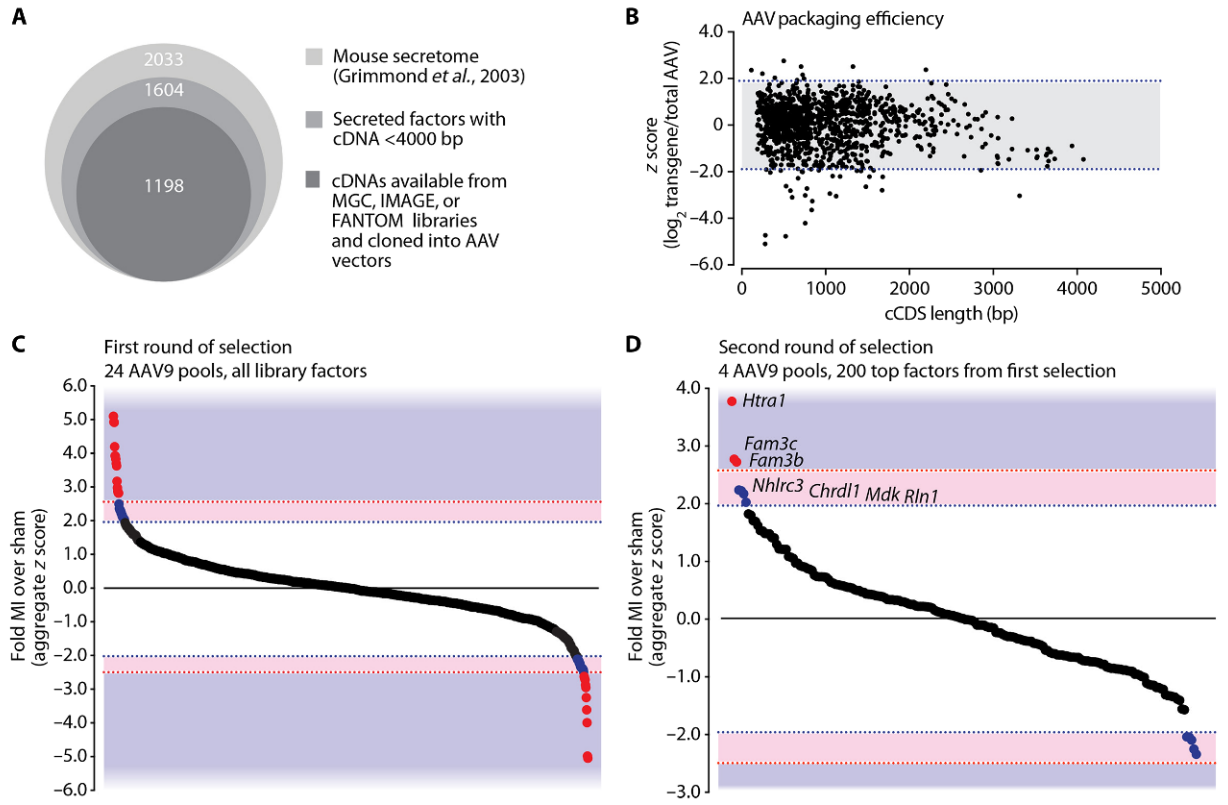

Fig. 2. AAV secretome library screening after myocardial infarction (MI). (**A**) Selection of cDNAs for the generation of the AAV mouse secretome collection. (**B**) Packaging efficiency of AAV clones after pooled production. The graph shows the cumulative *z* score distributions of all cDNA clones in the 24 AAV9 pools of the secretome library, as quantified in the vector lysates, plotted against the length of vector insert. cCDS, cDNA coding sequence. The total AAV insert length has additional 689 bp, which include the CMV promoter and poly A site, identical for all clones. (**C**) Cumulative results of the in vivo competitive screening of the 1198 AAV vectors of the FunSel library after MI. AAV9 vectors were organized into 24 pools, each composed of 50 different vectors. The waterfall plot shows the *z* scores for enrichment factors, arrayed by ascending the magnitude of effect. Each dot shows the relative enrichment of each factor, as detected by barcode abundance over control, undamaged hearts (sham), 3 weeks after administration (0, no selection; positive values, enrichment; negative values, negative selection). The pink- and violet-colored areas indicate *z* score ≥ ±1.96 and *z* score ≥ ±2.58, respectively. Individual results for each of the 24 pools are shown in fig. S2. (**D**) Waterfall plot showing the cumulative results obtained from the in vivo screening of the top 200 factors enriched in the first round of selection. Data are presented as in (B). Statistically selected top factors are in red (*z* score ≥ 2.58) or blue (*z* score ≥ 1.58).

We wanted to confirm the efficacy of the top selected factors once delivered as individual AAV9 vectors after MI. Adult female CD1 mice underwent surgical induction of MI and then received intramyocardial injections of AAV9 vectors (1×10^{11} vg per animal; $n = 8$ per group) expressing each of the top five genes (*Chrdl1*, *Fam3c*, *Fam3b*, *Htra1*, and *Nhlrc3*), *Mdk*, or a control vector containing an empty polylinker (AAV9-Control) into the infarct border zone (Fig. 3A). This resulted in efficient myocardial transduction and long-lasting transgene expression for each of the six tested AAV9 vectors, both after MI (fig. S5A) and also in healthy hearts, as investigated for Chrdl1, Fam3c, and Fam3b (fig. S5, B and C). The same vectors were also effective at driving transgene expression in isolated neonatal CMs [fig. S5 (D and E) for mRNA and protein amounts, respectively].

As assessed by echocardiography 15, 30, and 60 days after treatment, Chrdl1, Fam3c, and Fam3b were very effective at maintaining cardiac function and preventing post-MI cardiac dilatation [Fig. 3 (B and C), respectively]. Left ventricular ejection fraction (LVEF) was 47.7 ± 3.6%, 43.8 ± 2.7%, and 40.5 ± 2.8%, respectively, 60 days after MI and treatment, compared to 19.5 ± 2.7% in the AAV9-Control–injected animals ($P < 0.01$ in all three cases). At the same late time point, LV end-diastolic volume (LVEDV) was 66.2 ± 7.0, 70.0 ± 5.2, and 78.0 ± 2.7 μl for Chrdl1, Fam3c, and Fam3b, respectively, versus 124.6 ± 8.8 μl for control animals ($P < 0.01$ in all cases). Additional parameters of cardiac function are shown in fig. S6. Two other factors, Htra1 and Nhlrc3, were also effective in reducing dilatation (left ventricular end diastolic diameter, LVEDV) and partially improving function (left ventricular fractional shortening, LVFS, and LVEF), however less efficiently. All factors outperformed Mdk1.

Morphometric analysis on trichrome-stained heart sections after animal euthanasia at day 60 indicated that all the six investigated factors significantly preserved LV mass and reduced the fibrotic area (Fig. 3, D to G). Infarct size was 7.5 ± 0.8%, 10.9 ± 1.1%, and 13.5 ± 1.4% of LV for Chrdl1, Fam3c, and Fam3b, respectively, compared with 30.6 ± 1.3% for the AAV9-Control–treated animals ($P < 0.01$ in all cases; Fig. 3E).

Therapeutic effect of circulating cardioactive factors after MI

To evaluate whether circulating Chrdl1, Fam3b, and Fam3c can exert their protective function once reaching the heart from the circulation, as opposed to being expressed within the heart using viral

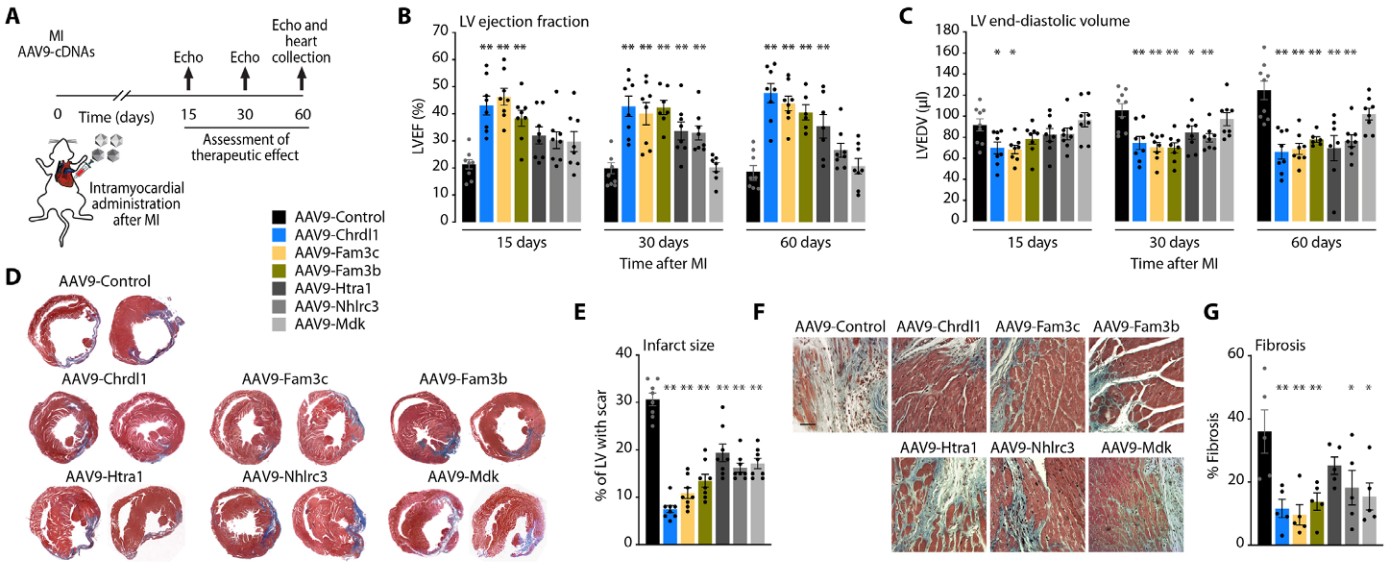

Fig. 3. Cardioprotective effect against MI of the FunSel top hits. (**A**) Experimental protocol. Transduction was performed with individual AAV9 vectors expressing Chrdl1, Fam3c, Fam3b, Mdk, Nhlrc3, or Htra1 (1×10^{11} vg per animal). (**B** and **C**) Echocardiographic analysis of infarcted mice at 15, 30, and 60 days after MI and the indicated treatments. Data are means ± SEM; $n = 8$ per group; $^{*}P < 0.05$ and $^{**}P < 0.01$ versus AAV9-Control; two-way ANOVA with Bonferroni post hoc correction. LVEF, left ventricular ejection fraction; LVEDV, left ventricular end-diastolic volume. (**D**) Representative images of Masson's trichrome stains of heart transverse sections 60 days after MI and vector injection. Fibrotic areas are stained blue. (**E**) Quantification of left ventricle (LV) infarct size. Data are means ± SEM; $n = 8$ per group; $^{**}P < 0.01$ versus AAV9-Control; one-way ANOVA with Bonferroni post hoc correction. (**F**) Representative images of ventricular fibrosis at higher magnification. Scale bar, 50 µM. (**G**) Quantification of tissue fibrosis in the infarct border zone. Data are means ± SEM; $n = 5$ per group; $^{*}P < 0.05$ and $^{**}P < 0.01$ versus AAV9-Control; one-way ANOVA with Bonferroni post hoc correction.

vectors, thus paving the way to their use as recombinant proteins, we designed a strategy in which each of the three factors was secreted from the liver into the blood. We generated liver-specific AAV vectors by cloning each factor's coding sequence under the control of the human α-1 antitrypsin (hAAT) promoter, which ensures exclusive expression in hepatocytes (*44*, *45*), and we packaged the vector DNAs using the liver-specific AAV8 (Fig. 4A). Each factor was tagged with a Flag epitope in the absence of available reliable, specific antibodies. The scheme of the experiment is shown in Fig. 4B. One week after direct intraparenchymal injection into the liver, transgene expression and protein release in the circulation were assessed by real-time PCR and Western blotting, respectively. Transgene expression was robust for all three factors (Fig. 4C), and each protein was detectable in both liver lysates and in serum (Fig. 4D). No expression of the factors was detected in the heart by reverse transcription PCR (Fig. 4C). Three days after assessment of effective protein secretion, animals were subjected to MI and then followed by echocardiography at days 15, 30, and 60 after MI. All the treated mice showed improvement in cardiac function and less-pronounced LV remodeling than control animals, similar to what was observed after AAV9 vector–mediated intracardiac transduction. In particular, the therapeutic effects of Chrdl1, Fam3c, and Fam3b were already evident 15 days after MI and were maintained for 2 months (LVEF: $P < 0.001$ for Chrdl1, Fam3c, and Fam3b versus AAV8-Control at 60 days; Fig. 4E). Negative cardiac remodeling was also prevented by each of the three factors (LVEDV: $P < 0.001$ for Chrdl1, Fam3c, and Fam3b versus AAV8-Control at 60 days; Fig. 4F).

In line with the protective effects of the three factors, the liver-treated mice developed smaller infarct scars, as assessed from trichrome-stained heart cross sections. Infarct size was significantly reduced compared to control animals ($P < 0.01$ for all three proteins; Fig. 4, G and H). Collectively, this set of data indicates that Chrdl1, Fam3c, and Fam3b can preserve cardiac integrity and function after MI when reaching the heart from the circulation.

Mechanisms of cardioprotection by Chrdl1

Next, we focused on Chdrl1 because this factor was particularly effective at both preserving muscularization and preventing negative cardiac remodeling after MI. Chrdl1 belongs to the Chordin family and acts as a BMP inhibitor in early cardiac development (*13*). No role has, so far, been reported for Chrdl1 in the adult heart. We started by investigating the effects of Chrdl1 in infarcted animals 1 month after the treatment. Consistent with the reduction in infarct size and prevention of pathological remodeling, CM cross-sectional area, a measurement for the compensatory hypertrophic response, was markedly blunted in the Chrdl1-treated animals and not different as in noninfarcted hearts (Fig. 5A).

Angiogenesis as measured by an increase in capillaries [$CD31^{+}$ or wheat germ agglutinin (WGA^{+}) vessels] or arterioles [α-smooth muscle actin (SMA^{+}) vessels] was not significantly different in the Chrdl1-treated hearts (Fig. 5B) compared to controls. We thus turned our attention to the events that occur at earlier times after MI. Consistent with a direct protective role in CM viability, we found that Chrdl1 markedly suppressed apoptotic cell death. Two days after MI, 30.1 ± 1.7% of cells were positive for terminal deoxynucleotidyl transferase–mediated deoxyuridine triphosphate nick end labeling (TUNEL) staining in the LV anterior wall of control animals versus 4.3 ± 0.6% in the animals treated with Chrdl1 ($P < 0.01$; Fig. 5C).

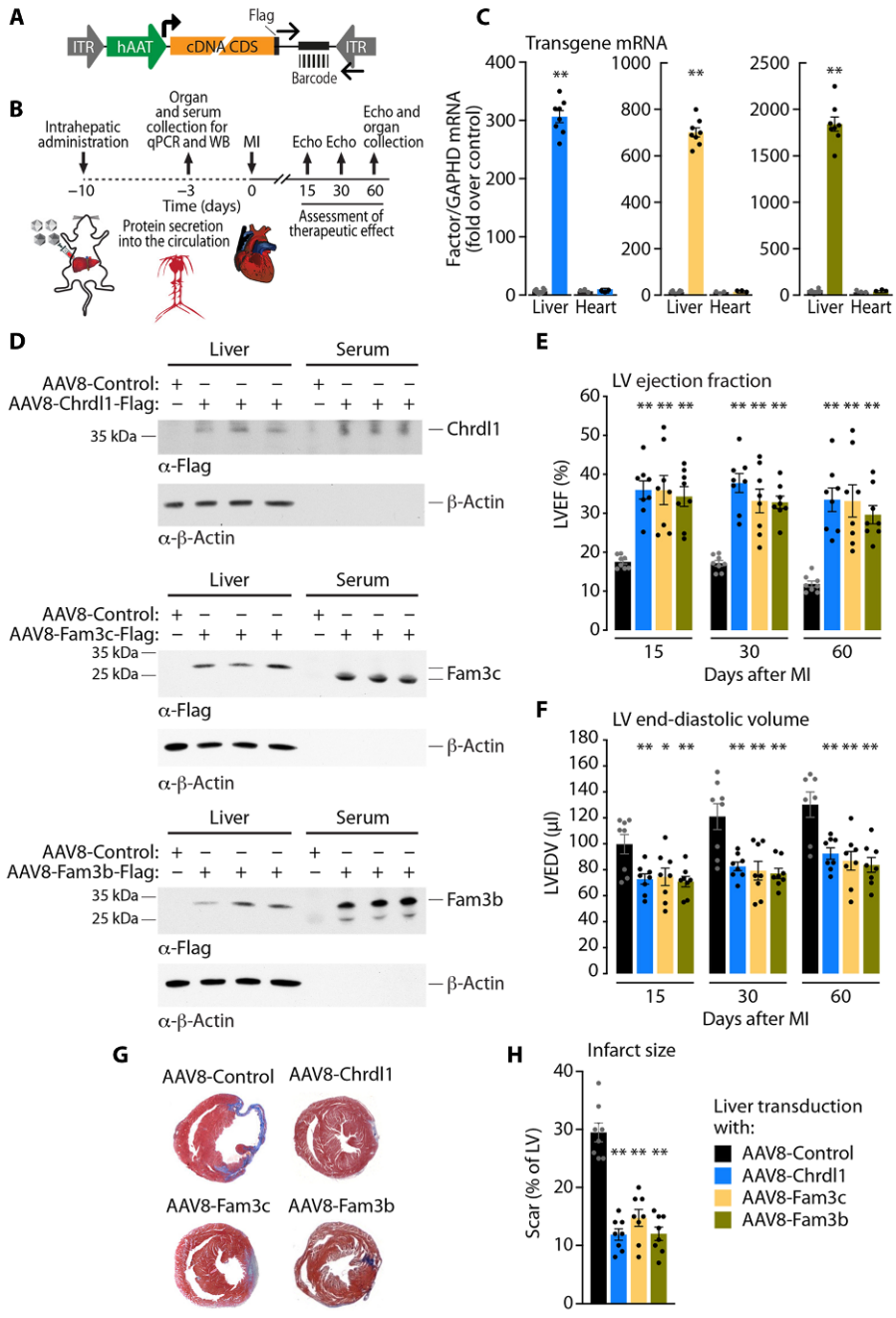

Fig. 4. Therapeutic effect of circulating cardioactive factors after MI. (**A**) Schematics of the pGG2 modified plasmid used for the generation of AAV8 vectors. Transgene CDSs are under the control of the human α1-antitrypsin (hAAT) promoter. (**B**) Outline of the strategy to assess therapeutic efficacy of the factors released into the circulation from the liver to mimic systemic administration of recombinant proteins. (**C**) Quantification of transgene expression in both liver and heart at day 7 after direct intrahepatic injection. Data are means ± SEM ($n = 8$ for liver and $n = 3$ for heart), normalized for glyceraldehyde phosphate dehydrogenase (GAPDH) and expressed over nontransduced; $^{**}P < 0.01$ versus sham; *t* test. (**D**) Representative Western blots for the detection of the Flag-tagged proteins in the liver and in serum 7 days after AAV8 administration. Paired samples (liver and serum) from three different animals per factor and one control are shown. Detection of the factors used an anti-Flag epitope antibody. In immunoblottings, Fam3c is commonly detected in two forms of different mass (*78*, *79*), the smaller of which appears to be secreted from the liver after transduction. (**E** and **F**) Echocardiographic analysis at the indicated time points after MI in animals treated with the indicated factors [color code as in (H)]. Data are means ± SEM; $n = 8$ per group; $^{*}P < 0.05$ and $^{**}P < 0.01$ versus AAV9-Control; two-way ANOVA with Bonferroni post hoc correction. (**G**) Representative images of Masson's trichrome stains of heart transverse sections 60 days after MI. Fibrotic areas are stained blue. (**H**) Quantification of LV infarct size. Data are means ± SEM; $n = 8$ per group; $^{**}P < 0.01$ versus AAV9-Control; one-way ANOVA with Bonferroni post hoc correction.

In the same hearts 2 days after infarction, we also found that Chrdl1 markedly stimulated CM autophagy. Both the conversion of LC3-I to LC3-II and the amount of Atg5 were significantly higher in the hearts of the treated animals ($P < 0.05$ and $P < 0.01$, respectively; Fig. 5D).

We were intrigued by the possibility that Chrdl1 exerted its cardioprotective activity by the stimulation of protective CM macroautophagy (hereafter referred to as autophagy) (*46*). We thus used AAV6 vectors to transduce neonatal rat ventricular CMs in vitro to express Chrdl1 (fig. S5, D and E). We found that Chrdl1 promoted evident formation of autophagosomes in CMs, as indicated by an increase in the number of LC3-positive vesicles 72 hours after transduction (Fig. 5E). This was consistent with increased amounts of the translipidated form of LC3 (LC3-II) and of Atg5, a factor that is essential for the first steps of autophagosome formation (Fig. 5F). To directly visualize the autophagic flux, we transduced CMs with an AAV6 vector expressing Chrdl1 and an additional vector expressing, in tandem, monomeric red fluorescent protein (mRFP), enhanced green fluorescent protein (EGFP), and the LC3 protein, derived from the ptfLC3 plasmid (*47*). This construct allows distinction of autophagosomes (both green and red; yellow) from autolysosomes (red only) because EGFP fluorescence is quenched in acidic autolysosomes (Fig. 5G). At 72 hours after AAV6 transduction, Chrdl1 induced an evident increase in autophagic flux (Fig. 5H).

Together, the results of these experiments are consistent with the conclusion that the cardioprotective effect exerted by Chrdl1 is mediated by the prevention of CM death and correlates with the induction of autophagy. Thus, we wondered whether the other two top factors selected by our screening, Fam3c and Fam3b, were also capable of inducing autophagy. We found that both factors, and particularly Fam3c, increased LC3 translipidation and Atg5 amounts both in vivo at 2 days after MI (fig. S7A) and in isolated CMs in vitro (fig. S7B). Fam3c was also particularly effective at inducing the formation of LC3-positive autophagosomal vesicles in CMs (fig. S7C) and stimulating autophagic flux (fig. S7D). Both Fam3c and Fam3b also protected CMs against apoptosis at 2 days after MI in vivo (fig. S7E).

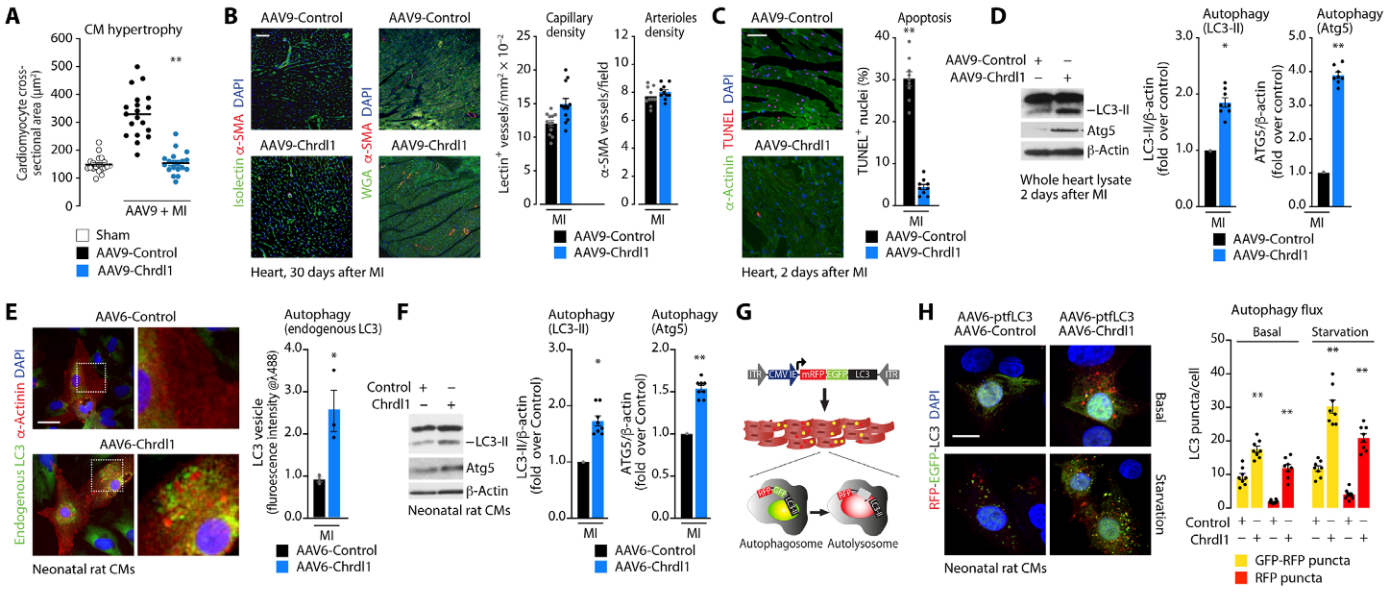

Fig. 5. Functional correlates of Chrdl1 cardioprotective activity. (**A**) Measurement of CM cross-sectional area after wheat germ agglutinin (WGA) staining of heart sections in infarcted mice injected with AAV9-Control or AAV9-Chrdl1. Sham animals were used as controls. At least 10 high-power fields per area from a minimum three slides per heart were analyzed to obtain the average regional cross-sectional area and regional myocyte nuclear density. The mean of values is shown. $^{**}P < 0.01$ versus control; one-way ANOVA with Bonferroni post hoc correction. (**B**) Capillary and arteriole density in infarcted hearts treated with the indicated vectors. The images on the left show immunofluorescence of isolectin or WGA and α-SMA. Data in the bar graphs on the right are means ± SEM; $n = 10$ high-power fields per area from a minimum three slides per heart. Scale bar, 100 μM. (**C**) TUNEL$^+$ nuclei in the peri-infarct region (representative images and quantification). Immediately after MI, animals were transduced with AAV9 vectors expressing the indicated factors; TUNEL analysis was performed 2 days after MI and treatment. Data are means ± SEM ($n = 8$); $^{**}P < 0.01$ versus AAV6-Control; one-way ANOVA with Bonferroni post hoc correction; the entire dataset also includes data in fig. S5E. Scale bar, 100 μM. (**D**) LC3 lipidation in the LVs of hearts transduced with the indicated AAV9 vectors at 2 days after MI (representative Western blotting images and densitometric analysis; the complete immunoblot and dataset are shown in fig S7A). Data are means ± SEM ($n = 8$); $^{*}P < 0.05$ and $^{**}P < 0.01$ versus AAV6-Control; one-way ANOVA with Bonferroni post hoc correction. (**E**) Left: Representative images of rat α-actinin$^+$ CMs (red) showing induction of LC3$^+$ vesicles (green) in response to AAV6-Chrdl1. Right: Quantification of CM-LC3$^+$ vesicles expressed as fluorescence intensity. Data are means ± SEM ($n = 3$ biological replicates). $^{*}P < 0.05$ versus AAV6-Control; one-way ANOVA with Bonferroni post hoc correction. Scale bar, 10 μM. (**F**) LC3 lipidation (conversion from LC3-I to LC3-II) and amount of Atg5 in rat CMs treated with the indicated vectors after serum starvation (0.1% FBS) for 12 hours. Representative Western blot (left) and quantification (right); the complete immunoblot and dataset are shown in fig. S7B. Data are means ± SEM; $n = 8$; $^{*}P < 0.05$ and $^{**}P < 0.01$ versus AAV6-Control; one-way ANOVA with Bonferroni post hoc correction. (**G**) Schematic of the AAV6-LC3-GFP-RFP reporter vector. Autophagosome and autolysosome are shown as yellow and red dots, respectively. (**H**) Autophagic flux in primary rat CMs (representative images and quantification). Cells were cotransduced with AAV6-mRFP-EGFP-LC3 and an AAV6 expressing Chrdl1, Fam3c, or Fam3B. Autophagosomes appear yellow in the merged image, and autolysosomes appear red. Cells were kept in basal and starvation conditions. Data are means ± SEM; $n = 3$ biological replicates; at least 30 cells were quantified; $^{**}P < 0.01$ versus AAV6-Control; two-way ANOVA with Bonferroni post hoc correction. Data from Fam3c and Fam3b that were included in the statistical analysis are in fig. S5D. Scale bar, 10 μM

These findings reinforce the conclusion that the induction of autophagy is a major protective mechanism in the infarcted heart.

Mouse Chrdl1, Fam3c, and Fam3b share 85.1, 92.9, and 65.5% amino acid identity, respectively, with their respective human homologous proteins. Thus, we wondered whether the biological effects of the three factors were also exerted by the respective human proteins. We found that all three human recombinant proteins enhanced LC3 translipidation in both rat (fig. S8, A and B) and mouse (fig. S8, C and D) CMs, as well as autophagic flux in rat CMs treated with chloroquine (fig. S8, E and F). The human recombinant proteins were also effective at inducing autophagic flux in human induced pluripotent stem (iPS) cell–derived human CMs (fig. S8, G and H). This maintained cross-species activity has obvious interest for clinical translation.

BMP4 inhibits autophagy and is inactivated by Chrdl1

Next, we wanted to understand the molecular mechanisms by which Chdrl1 exerted its function. The members of the Chordin family are known to bind extracellular BMPs and prevent their receptor interaction (*13*). Consistent with this information, we found that activation of the BMP pathway by BMP4 (as determined by phosphorylation of the SMAD1/5/8 signal transduction proteins) was inhibited by AAV6-Chrdl1 in a dose-dependent manner (Fig. 6, A and B). More than 90% of cells treated with BMP4 (10 ng/ml) showed nuclear localization of SMAD1/5/8, whereas this percentage was reduced to 55% in cells expressing Chrdl1 (fig. S9, A and B). These experiments revealed the previously unappreciated effect of BMP4 in depressing basal autophagy, resulting in lower amounts of translipidated LC3-II and Atg5 in CMs treated with this factor (Fig. 6, C and D). In contrast, autophagy was increased in CMs transduced with AAV6-Chrdl1, which blunted the negative BMP4 effect. The effect of Chrdl1 was comparable to that of dorsomorphin, an inhibitor of BMP type I receptors (*48*). Consistent with these findings, both the number of endogenous LC3-positive vesicles (Fig. 6E) and autophagic flux (Fig. 6, F and G) were reduced by BMP4 and rescued by Chrdl1 in primary CMs.

Chrdl1 inhibits TGF-β1–induced cardiac fibrosis and myofibroblast transdifferentiation

In addition to CM protection and consequent maintenance of cardiac muscle mass, we also noticed that the infarcted hearts treated

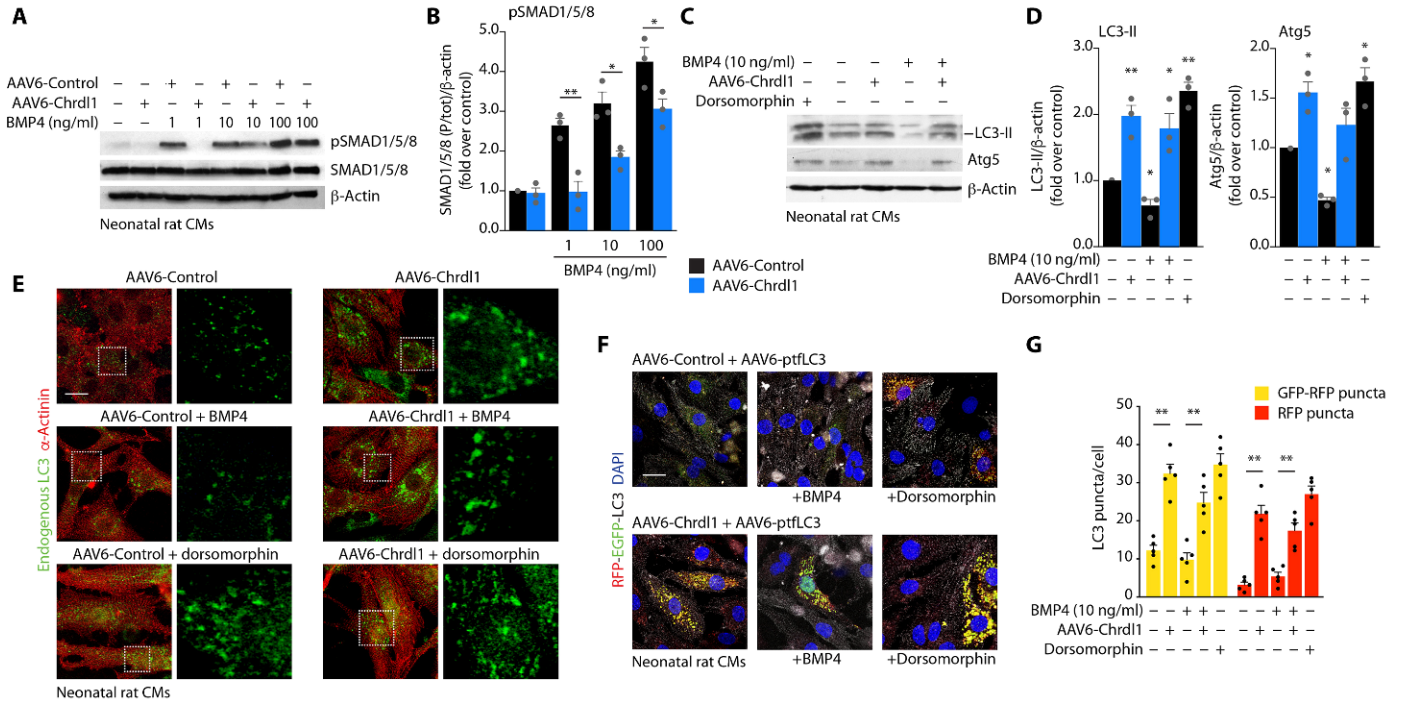

Fig. 6. Chrdl1 reduces BMP4-induced SMAD1/5/8 activation in CMs. (**A** and **B**) Representative Western blotting and densitometric analysis showing SMAD1/5/8 phosphorylation in rat CMs stimulated with increasing doses of BMP4 for 30 min after cell transduction with AAV6-Control or AAV6-Chrdl1, respectively. Data are means ± SEM; $n = 3$ biological replicates per condition; $^{*}P < 0.05$ and $^{**}P < 0.01$ versus AAV6-Control; t test. (**C** and **D**) LC3 lipidation and Atg5 expression (representative blot and densitometric quantification, respectively) in rat CMs expressing Chrdl1 and treated with BMP4 or the SMAD inhibitor dorsomorphin (10 μM) 12 hours after treatment. Data are normalized over β-actin and expressed as fold over untreated. Data are means ± SEM; $n = 3$ replicates; $^{*}P < 0.05$ and $^{**}P < 0.01$ versus AAV6-Control; one-way ANOVA with Bonferroni post hoc correction. (**E**) Confocal microscopy images showing LC3-positive vesicles in rat CMs expressing Chrdl1 and treated with BMP4 (10 ng/ml) or dorsomorphin (10 μM). α-Actinin, red; LC3, green. Scale bar, 10 μM. (**F** and **G**) Autophagic flux (representative confocal microscopy images and quantification of vesicles, respectively) in primary rat CMs transduced with AAV6-mRFP-EGFP-LC3 and, 48 hours later, starved and treated for 12 hours with BMP4 (100 ng/ml) or dorsomorphin (10 μm). Early autophagic vesicles (autophagosomes) are yellow, and late vesicles (autolysosomes) are red. Data are means ± SEM; $n = 3$ replicates; $^{**}P < 0.01$ versus control; two-way ANOVA with Bonferroni post hoc correction. At least 30 cells were quantified per group. Scale bar, 10 μM

with Chrdl1 had a smaller volume, which was indicative of blunted maladaptive remodeling (Fig. 3C), and showed reduced interstitial fibrosis (Fig. 3G). This was suggestive of an effect of Chrdl1 extending beyond its function in CMs. A master factor regulating the myocardial response to damage is TGF-β, which stimulates transdifferentiation of cardiac fibroblasts into α-SMA–positive myofibroblasts, followed by extracellular matrix deposition (*49*). Given the broad cross-talk and overlap between the BMP and TGF-β pathways, we wondered whether Chrdl1 might also directly affect TGF-β signal transduction in fibroblasts.

We started by transfecting mouse NIH-3T3 fibroblasts with pAAV-Chrdl1, followed by cell treatment with TGF-β1 for 30 min 2 days after transfection. SMAD2/3 phosphorylation, an established readout for TGF-β pathway activation, was notably reduced in Chrdl1-transfected cells [representative blots and quantification in Fig. 7 (A and B), respectively]. This was also confirmed by visualizing SMAD2/3 translocation into the nucleus in response to TGF-β. Cell treatment with TGF-β (10 ng/ml) determined nuclear localization of SMAD2/3 in >90% of the cells, whereas this percentage was reduced to about 50% when cells had been transfected with pAAV-Chrdl1 [representative images and quantification in fig. S10 (A and B), respectively]. An inhibitory effect of Chrdl1 on SMAD2/3 nuclear translocation was also observed in primary cardiac fibroblasts treated with recombinant Chrdl1 (fig. S10C). Last, we also monitored activation of the TGF-β1 pathway using a reporter gene assay. NIH-3T3 fibroblasts stably expressing luciferase under the control of a synthetic promoter containing 12 basal SMAD3-CAGA binding sites [CAGA-luc (*50*); scheme in Fig. 7C] were stimulated by increasing doses of TGF-β1 after treatment with recombinant Chrdl1. Transcription of the reporter gene, which showed dose-dependent activation in response to TGF-β1, was blunted in Chrdl1-treated cells at all TGF-β1 doses (Fig. 7D). The TGF-β1 chemical inhibitor SB431542 (*51*) served as a positive control for these experiments.

Inhibition of SMAD2/3 phosphorylation and nuclear translocation, together with impairment of TGF-β1–induced transcriptional activation, are concordant in indicating that Chrdl1 acts as a TGF-β1 inhibitor. We could detect a physical interaction between the two proteins by transfecting human embryonic kidney (HEK) 293 cells with a Flag-Chrdl1 expression vector, followed by addition of 0.2 mg of TGF-β1 to the cell supernatant for 1 hour at 4°C. The immunoprecipitate obtained with anti-Flag magnetic beads also contained TGF-β1 (Fig. 7E).

Treatment of primary mouse cardiac fibroblasts for three consecutive days with increasing doses of TGF-β1 (from 1 to 50 ng/ml; experimental scheme in Fig. 7F) induced a dose-dependent increase in collagen I deposition (as assessed using a specific antibody) and myoblast transdifferentiation (positivity for α-SMA). Treatment with recombinant Chrdl1 markedly reduced this effect (Fig. 7, G to I).

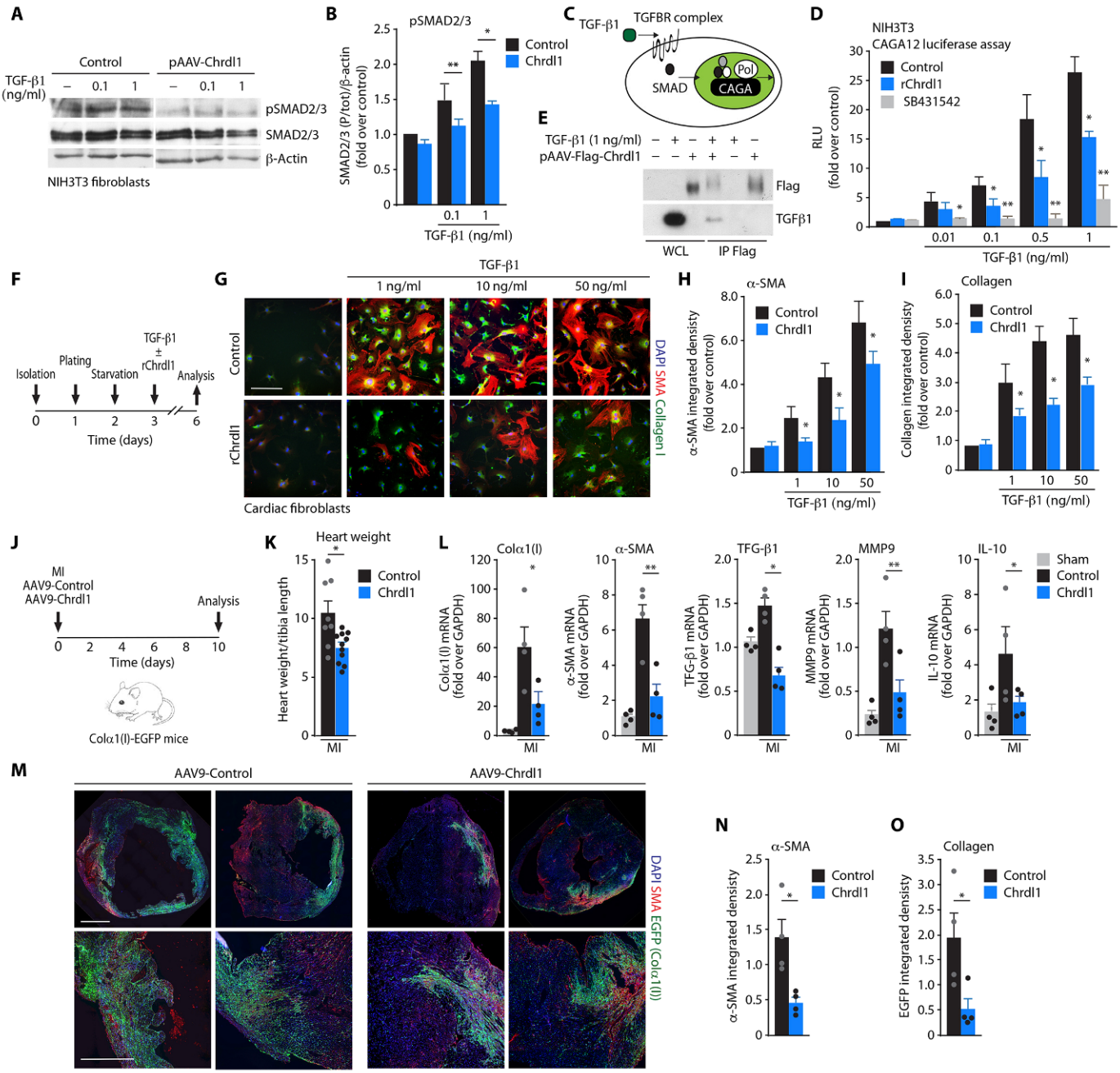

Fig. 7. Chrdl1 reduces TGF-β1–induced SMAD2/3 activation and cardiac fibrosis. (**A** and **B**) Representative Western blotting and densitometric analysis showing SMAD2/3 phosphorylation in NIH-3T3 fibroblasts stimulated with increasing doses of TGF-β1 for 30 min after control or pChrdl1 transfection, respectively. Data are means ± SEM; $n = 3$ biological replicates per condition; $^{*}P < 0.05$ and $^{**}P < 0.01$ versus control; *t* test. (**C**) CAGA luciferase assay in NIH-3T3 cells stably expressing a luciferase reporter under the control of the SMAD-CAGA responsive element. (**D**) Results of CAGA luciferase assay after stimulation with increasing doses of TGF-β1 in association with Chrdl1 or the TGF-β1 inhibitor SB431542 (1 μM). Data are means ± SEM; $n = 3$ biological replicates per condition; $^{*}P < 0.05$ and $^{**}P < 0.01$ versus control; one-way ANOVA with Bonferroni post hoc correction. (**E**) Immunoprecipitation of Flag-Chrdl1 with TGF-β1. Recombinant TGF-β1 was added to the supernatant of HEK293T cells expressing Flag-Chrdl1 for 1 hour, followed by immunoprecipitation (IP) with anti-Flag beads. (**F**) Outline of the experiment aimed at assessing conversion of primary cardiac fibroblasts into myofibroblast by TGF-β1 stimulation. (**G** to **I**) Effect of recombinant Chrdl1 on TGF-β1–induced myofibroblast conversion (representative immunofluorescence and quantification of α-SMA and collagen mean fluorescence intensity, respectively). α-SMA, red; collagen I, green; nuclei, blue. Data are means ± SEM; $n = 3$ biological replicates per dose; $^{*}P < 0.05$ and $^{**}P < 0.01$ versus control; *t* test. (**J**) Outline of the in vivo experiments in Colα1(I)-EGFP mice. Animals were injected with AAV9-Control or AAV9-Chrdl1 and were euthanized 10 days after MI. (**K**) Heart weight/tibia length ratio of Colα1(I)-EGFP mice 10 days after MI ($n = 8$). Data are means ± SEM; $^{*}P < 0.05$ versus control; *t* test. Scale bar, 50 μM. (**L**) Expression of the indicated factors after intracardiac injection of AAV9-Control or AAV9-Chrdl1 in infarcted mice ($n = 4$). The amounts in sham animals (no MI; $n = 4$) are shown for reference. Data are means ± SEM; $^{*}P < 0.05$ and $^{**}P < 0.01$ versus control; *t* test. (**M** to **O**) Effect of Chrdl1 after MI in Colα1(I)-EGFP mice [representative images of heart sections and quantification of α-SMA and Colα1(I) cell mean fluorescence intensity, respectively]. α-SMA, red; EGFP [Colα1(I)] cells, green; nuclei, blue. Data are means ± SEM; $n = 4$; $^{*}P < 0.05$ versus control; *t* test. Scale bar, 1 mm.

Similar results were obtained using NIH3T3 fibroblasts transfected with Chrdl1 (fig. S10D).

Last, we investigated the effect of Chrdl1 on the fibrotic response in vivo after MI. We took advantage of type I collagen α1 [Colα1(I)]–EGFP mice, a transgenic mouse line in which EGFP is expressed in fibroblasts under the control of the Colα1(I) promoter/enhancers (*52*). Mice were treated by intramyocardial injection of AAV9-Chrdl1 or AAV9-Control after MI (experimental scheme in Fig. 7J). Ten days after treatment, the Chrdl1-transduced hearts were not dilated, and their weight was smaller than that of the control animals (Fig. 7K). The expression of Colα1(I), α-SMA, TGF-β1, MMP9 (matrix metalloproteinase 9), and IL-10, all markers of fibrotic deposition and myofibroblast transition, were reduced (Fig. 7L), whereas the MI scars were smaller and more compact, showing attenuated fibrosis and reduced collagen I and α-SMA expression (Fig. 7, M to O).

Together, these results confirm that Chrdl1, in addition to its proautophagic and prosurvival function in CMs, also acts on cardiac fibroblasts after MI by binding and inhibiting TGF-β1. This interaction results in attenuated fibrotic response and decreased pathological remodeling.

DISCUSSION

In genetic research, several ground-breaking findings have resulted not from candidate gene studies but through unbiased functional screening or selection of genetic libraries in cultured cells. For example, the discovery of oncogenes in the 1980s (*53*), CXCR-4 as an HIV-1 coreceptor in the 1990s (*54*), and iPS-inducing factors in the 2000s (*55*) all derive from cell-based, functional studies. However, although these in vitro functional approaches generate essential biological information, often with important upshots on drug discovery, they cannot predict the in vivo relevance of the selected molecules. The possibility of screening nucleic acid libraries for a given function directly in vivo thus offers a unique opportunity to identify novel therapeutic factors, in the absence of any a priori, possibly biased, information on their actual mechanism of action.

The efficient delivery of arrayed genetic libraries in vivo for functional selection, especially in postmitotic tissues, remains a major problem. Transduction of nonreplicating cells in vivo, persistence of transgene expression for indefinite periods of time, and lack of relevant inflammatory or immune response (*56*) render AAV vectors excellent tools for this purpose. We observed that the administration of these vectors after MI results in transgene expression as early as 2 hours after injection to reach a plateau after 12 hours. This kinetics, which is accelerated by tissue damage compared to that observed in uninjured muscle (*57*, *58*), appears to be suitable for the selection of cardioprotective factors acting rapidly after MI. In terms of multiplicity of infection, the efficiency of FunSel in selecting functionally protective factors is favored by performing transduction with a relatively low number of vectors per cell. In any case, should a beneficial factor be mixed with other neutral factors in the same cell, still, the cell would become selected and the beneficial factor would be enriched over the others, because the neutral factors would be different in each transduced cell (*14*).

FunSel is unbiased, because it is agnostic with regard to factors and their mechanisms of action; competitive, because it is based on an in vivo competition between beneficial, neutral, and detrimental factors; iterative, because vectors can be selected by progressive rounds; and comparative, because it permits ranking of the selected molecules for efficacy. The identified factors act at the single-cell level by conferring individual cell protection, which can be achieved directly or indirectly, for example, by inducing intrinsic cell survival mechanisms directly or modulating the cell environment (e.g., inflammation or angiogenesis). Our original proof-of-concept FunSel study (*14*) was performed in the skeletal muscle, with a limited number of vectors and with iterative rounds of selection in which progressive factor enrichment was analyzed by resolving PCR products by electrophoresis. Instead, this cardiac version of FunSel here is based on a novel, large cDNA library from the mouse secretome, in which all the vectors are barcoded. This allows detection of the selected factors after a single round of screening by NGS. In this format, FunSel can be easily applied to the selection of protective factors in any other organ in which a relevant animal model for tissue degeneration is available and in which cells can be transduced by AAV vectors. FunSel is based on the relative number of sequencing reads of the AAV vectors that persist in the transduced tissue after damage. As these vectors do not integrate into the cellular genome nor replicate autonomously, FunSel does not screen for factors that induce cardiac regeneration based on endogenous CM proliferation. Another limitation is that some of the factors that exert a protective role might be overlooked in the screening, for example, because of their random inclusion in pools with other factors with stronger activity.

Among the top 10 genes that emerged from the screening, there were *Mdk* (*59*, *60*) and pleiotrophin (*61*), two proteins that were previously described as protective for the myocardium. To the best of our knowledge, a cardioprotective role has not yet been reported for the top five hits in our screening (*Chrdl1*, *Fam3c*, *Fam3b*, *Htra1*, and *Nhlrc3*). The overexpression of each of these five factors significantly preserved cardiac function and morphology and prevented pathological remodeling.

Chrdl1 is a BMP4 antagonist reported to act in the developing embryo (*13*) but having no recognized role itself in cardiac biology. BMP4, instead, is essential for atrioventricular septation and heart development, whereas its expression in the adult heart is known to be detrimental, leading to CM apoptosis, hypertrophy, and fibrosis (*62*). This information is consistent with the results of our experiments, which show that Chrdl1 directly binds BMP4, prevents SMAD1/5/8 activation, and protects CMs.

Fam3c and Fam3b are two members of the Fam3 (*63*, *64*). Fam3b, also known as PANcreatic DERived factor (PANDER), is highly expressed in the pancreas, where it participates in regulation of glucose homeostasis and β cell function (*22*, *65*, *66*). Fam3c, also known as IL-like epithelial-to-mesenchymal (EMT) transition inducer, is instead expressed ubiquitously and known to modulate inner ear cell proliferation (*23*), osteogenic differentiation (*67*), and EMT (*68*). Restoration of Fam3c expression in the liver of obese diabetic mice improves insulin resistance and reduces fatty liver degeneration (*69*).

Our experiments disclose that the induction of CM autophagy is a common mechanism of action for Chrdl1, Fam3c, and Fam3b in the heart and reinforce the notion that autophagy exerts a protective role after MI and other forms of cardiac damage (*70*). In postmitotic myocytes, autophagy maintains cardiac energy homeostasis and preserves cell vitality and function, thus preventing HF (*71*, *72*). In the acute phase after MI, this process is crucial to prevent ischemia/reperfusion-induced cell death (*73*). Chrdl1, Fam3c, and Fam3b are among the first cytokines found to pharmacologically stimulate this protective process.

Other BMP inhibitors present in our AAV library in addition to Chrdl1, including Chrdl2, Gremlin1 and Gremlin2, and Cerberus, scored markedly less effective or not effective at all at cardioprotection in our screening. This suggests that the cardioprotective effect of Chrdl1 could be exerted through additional mechanisms besides BMP4 inhibition. We found that extracellular Chrdl1 also acted on cardiac fibroblasts by blocking TGF-β1, a major inducer of fibrosis through the induction of fibroblast migration and their differentiation into myofibroblasts (*74*, *75*). Multiple lines of evidence indicate that the persistent activation of myofibroblasts leads to detrimental fibrosis in several organs, including the heart. Thus, an attenuated fibrotic response ensuing from reduced myofibroblast generation might well explain the decreased pathological remodeling we observed in our Chrdl1-treated hearts. Htra1, another of the top five factors selected by cardiac FunSel, is also a serine protease (*76*) that was reported to inhibit neuronal TGF-β and promote neuron survival (*77*). Together, these findings underline the potential of FunSel to select for tissue-protective factors that act in vivo through pleiotropic mechanisms and on different cell types, a condition that would be hardly reproducible in in vitro screening assays.

Functional selection of genes expressing secreted molecules offers important translational perspectives, as the identified factors could be administered as recombinant proteins, which can be properly dosed. Our observation that Chrdl1, Fam3c, and Fam3b maintain their cardioprotective activity when expressed from the liver provides a relevant proof of principle in this respect. On the basis of these results, we envisage the possible systemic administration of the cardioprotective protein immediately after MI and in anticipation of revascularization, with the intent to spare the myocardium from death due to, first, ischemia and, later, reperfusion. Further extensive experimentation will be required to first generate effective recombinant variants of these proteins and then assess their pharmacological profiles, dose, and route of administration in suitable small- and large-animal models to eventually move to efficacy studies.

MATERIALS AND METHODS

Study design

The primary objective of the study was to develop a method for the in vivo selection of factors exerting a protective function and to apply this method to the heart in mice with MI, based on the assumption that CMs expressing a beneficial factor would preferentially survive acute ischemia. Factors were selected from a barcoded library of AAV vectors that included 1198 cDNAs, each encoding for a different secreted factor. After selection induced by coronary artery ligation, the effect exerted by each factor was scored by counting the number of sequence reads of its barcode (positive factors have an increased number of reads). The best-performing factors were then verified by individual administration to the heart, in the form of AAV vectors, after MI. For these experiments, animals were randomly assigned to treatment or control groups. Animals showing a sign of distress or pain after surgery were euthanized. All the other animals, including outliers, were included in the analysis. Animal group size was determined according to prior power calculations. All mouse phenotyping was performed blinded. Library screening and mouse experiments were performed once. The secondary objective of the study was to study the mechanisms of action of the identified top factors. This involved experiments in primary neonatal mouse and rat CMs and human CMs from iPS cells. For immunofluorescence and molecular studies, sample size was estimated on the basis of known variability of the assays used. Sample sizes, replicates, and statistical methods are specified in the figure legends and the "Statistical analysis" section.

Statistical analysis

All data related to the individual characterization of candidate genes are expressed as mean of biological replicates ± SEM. Statistical analysis was performed using Prism software (GraphPad 9.0). $P < 0.05$ or lower was considered statistically significant. Pairwise comparison between groups was performed using the Student's t test. One-way analysis of variance (ANOVA) and Tukey's post hoc tests were used to compare multiple groups. Analysis of morphological and functional measurements at different time points among groups was performed using two-way ANOVA for repeated measurements, followed by pairwise post hoc analysis. Individual subject-level data are provided in data file S1.

SUPPLEMENTARY MATERIALS

www.science.org/doi/10.1126/scitranslmed.abo0699
Materials and Methods
Figs. S1 to S10
Tables S1 to S3
Data file S1
MDAR Reproducibility Checklist

View/request a protocol for this paper from *Bio-protocol*.

REFERENCES AND NOTES

1. GBD 2017 Disease and Injury Incidence and Prevalence Collaborators, Global, regional, and national incidence, prevalence, and years lived with disability for 354 diseases and injuries for 195 countries and territories, 1990–2017: A systematic analysis for the Global Burden of Disease Study 2017. *Lancet* **392**, 1789–1858 (2018).
2. E. J. Birks, Molecular changes after left ventricular assist device support for heart failure. *Circ. Res.* **113**, 777–791 (2013).
3. M. G. Crespo-Leiro, S. D. Anker, A. P. Maggioni, A. J. Coats, G. Filippatos, F. Ruschitzka, R. Ferrari, M. F. Piepoli, J. F. Delgado Jimenez, M. Metra, C. Fonseca, J. Hradec, O. Amir, D. Logeart, U. Dahlstrom, B. Merkely, J. Drozdz, E. Goncalvesova, M. Hassanein, O. Chioncel, M. Lainscak, P. M. Seferovic, D. Tousoulis, A. Kavoliuniene, F. Fruhwald, E. Fazlibegovic, A. Temizhan, P. Gatzov, A. Erglis, C. Laroche, A. Mebazaa; Heart Failure Association (HFA) of the European Society of Cardiology (ESC), European Society of Cardiology Heart Failure Long-Term Registry (ESC-HF-LT): 1-Year follow-up outcomes and differences across regions. *Eur. J. Heart Fail.* **18**, 613–625 (2016).
4. C. E. Murry, H. Reinecke, L. M. Pabon, Regeneration gaps. *J. Am. Coll. Cardiol.* **47**, 1777–1785 (2006).
5. G. Ambrosio, I. Tritto, Reperfusion injury: Experimental evidence and clinical implications. *Am. Heart J.* **138**, S69–S75 (1999).
6. O. Bergmann, R. D. Bhardwaj, S. Bernard, S. Zdunek, F. Barnabe-Heider, S. Walsh, J. Zupicich, K. Alkass, B. A. Buchholz, H. Druid, S. Jovinge, J. Frisen, Evidence for cardiomyocyte renewal in humans. *Science* **324**, 98–102 (2009).
7. B. Ibanez, G. Heusch, M. Ovize, F. Van de Werf, Evolving therapies for myocardial ischemia/reperfusion injury. *J. Am. Coll. Cardiol.* **65**, 1454–1471 (2015).
8. A. Skyschally, R. Schulz, G. Heusch, Pathophysiology of myocardial infarction: Protection by ischemic pre- and postconditioning. *Herz* **33**, 88–100 (2008).
9. P. Heusch, F. Nensa, G. Heusch, Is MRI really the gold standard for the quantification of salvage from myocardial infarction? *Circ. Res.* **117**, 222–224 (2015).
10. D. J. Hausenloy, R. K. Kharbanda, U. K. Moller, M. Ramlall, J. Aaroe, R. Butler, H. Bulluck, T. Clayton, A. Dana, M. Dodd, T. Engstrom, R. Evans, J. F. Lassen, E. F. Christensen, J. M. Garcia-Ruiz, D. A. Gorog, J. Hjort, R. F. Houghton, B. Ibanez, R. Knight, F. K. Lippert, J. T. Lonborg, M. Maeng, D. Milasinovic, R. More, J. M. Nicholas, L. O. Jensen, A. Perkins, N. Radovanovic, R. D. Rakhit, J. Ravkilde, A. D. Ryding, M. R. Schmidt, I. S. Riddervold, H. T. Sorensen, G. Stankovic, M. Varma, I. Webb, C. J. Terkelsen, J. P. Greenwood, D. M. Yellon, H. E. Botker; CONDI-2/ERIC-PPCI Investigators, Effect of remote ischaemic conditioning on clinical outcomes in patients with acute myocardial infarction (CONDI-2/ERIC-PPCI): A single-blind randomised controlled trial. *Lancet* **394**, 1415–1424 (2019).
11. J. T. Lee, R. E. Ideker, K. A. Reimer, Myocardial infarct size and location in relation to the coronary vascular bed at risk in man. *Circulation* **64**, 526–534 (1981).
12. C. E. Rochitte, C. F. Azevedo, The myocardial area at risk. *Heart* **98**, 348–350 (2012).

13. N. Nakayama, C. E. Han, S. Scully, R. Nishinakamura, C. He, L. Zeni, H. Yamane, D. Chang, D. Yu, T. Yokota, D. Wen, A novel chordin-like protein inhibitor for bone morphogenetic proteins expressed preferentially in mesenchymal cell lineages. *Dev. Biol.* **232**, 372–387 (2001).
14. G. Ruozi, F. Bortolotti, A. Falcione, M. Dal Ferro, L. Ukovich, A. Macedo, L. Zentilin, N. Filigheddu, G. Gortan Cappellari, G. Baldini, M. Zweyer, R. Barazzoni, A. Graziani, S. Zacchigna, M. Giacca, AAV-mediated in vivo functional selection of tissue-protective factors against ischaemia. *Nat. Commun.* **6**, 7388 (2015).
15. F. Bortolotti, G. Ruozi, A. Falcione, S. Doimo, M. Dal Ferro, P. Lesizza, L. Zentilin, L. Banks, S. Zacchigna, M. Giacca, In vivo functional selection identifies cardiotrophin-1 as a cardiac engraftment factor for mesenchymal stromal cells. *Circulation* **136**, 1509–1524 (2017).
16. S. M. Grimmond, K. C. Miranda, Z. Yuan, M. J. Davis, D. A. Hume, K. Yagi, N. Tominaga, H. Bono, Y. Hayashizaki, Y. Okazaki, R. D. Teasdale; RIKEN GER Group; GSL Members, The mouse secretome: Functional classification of the proteins secreted into the extracellular environment. *Genome Res.* **13**, 1350–1359 (2003).
17. W. Nickel, C. Rabouille, Mechanisms of regulated unconventional protein secretion. *Nat. Rev. Mol. Cell Biol.* **10**, 148–155 (2009).
18. R. L. Strausberg, E. A. Feingold, R. D. Klausner, F. S. Collins, The mammalian gene collection. *Science* **286**, 455–457 (1999).
19. R. L. Strausberg, E. A. Feingold, L. H. Grouse, J. G. Derge, R. D. Klausner, F. S. Collins, L. Wagner, C. M. Shenmen, G. D. Schuler, S. F. Altschul, B. Zeeberg, K. H. Buetow, C. F. Schaefer, N. K. Bhat, R. F. Hopkins, H. Jordan, T. Moore, S. I. Max, J. Wang, F. Hsieh, L. Diatchenko, K. Marusina, A. A. Farmer, G. M. Rubin, L. Hong, M. Stapleton, M. B. Soares, M. F. Bonaldo, T. L. Casavant, T. E. Scheetz, M. J. Brownstein, T. B. Usdin, S. Toshiyuki, P. Carninci, C. Prange, S. S. Raha, N. A. Loquellano, G. J. Peters, R. D. Abramson, S. J. Mullahy, S. A. Bosak, P. J. McEwan, K. J. McKernan, J. A. Malek, P. H. Gunaratne, S. Richards, K. C. Worley, S. Hale, A. M. Garcia, L. J. Gay, S. W. Hulyk, D. K. Villalon, D. M. Muzny, E. J. Sodergren, X. Lu, R. A. Gibbs, J. Fahey, E. Helton, M. Ketteman, A. Madan, S. Rodrigues, A. Sanchez, M. Whiting, A. Madan, A. C. Young, Y. Shevchenko, G. G. Bouffard, R. W. Blakesley, J. W. Touchman, E. D. Green, M. C. Dickson, A. C. Rodriguez, J. Grimwood, J. Schmutz, R. M. Myers, Y. S. Butterfield, M. I. Krzywinski, U. Skalska, D. E. Smailus, A. Schnerch, J. E. Schein, S. J. Jones, M. A. Marra; Mammalian Gene Collection (MGC) Program Team, Generation and initial analysis of more than 15,000 full-length human and mouse cDNA sequences. *Proc. Natl. Acad. Sci. U.S.A.* **99**, 16899–16903 (2002).
20. G. Lennon, C. Auffray, M. Polymeropoulos, M. B. Soares, The I.M.A.G.E. Consortium: An integrated molecular analysis of genomes and their expression. *Genomics* **33**, 151–152 (1996).
21. P. Carninci, T. Kasukawa, S. Katayama, J. Gough, M. C. Frith, N. Maeda, R. Oyama, T. Ravasi, B. Lenhard, C. Wells, R. Kodzius, K. Shimokawa, V. B. Bajic, S. E. Brenner, S. Batalov, A. R. Forrest, M. Zavolan, M. J. Davis, L. G. Wilming, V. Aidinis, J. E. Allen, A. Ambesi-Impiombato, R. Apweiler, R. N. Aturaliya, T. L. Bailey, M. Bansal, L. Baxter, K. W. Beisel, T. Bersano, H. Bono, A. M. Chalk, K. P. Chiu, V. Choudhary, A. Christoffels, D. R. Clutterbuck, M. L. Crowe, E. Dalla, B. P. Dalrymple, B. de Bono, G. Della Gatta, D. di Bernardo, T. Down, P. Engstrom, M. Fagiolini, G. Faulkner, C. F. Fletcher, T. Fukushima, M. Furuno, S. Futaki, M. Gariboldi, P. Georgii-Hemming, T. R. Gingeras, T. Gojobori, R. E. Green, S. Gustincich, M. Harbers, Y. Hayashi, T. K. Hensch, N. Hirokawa, D. Hill, L. Huminiecki, M. Iacono, K. Ikeo, A. Iwama, T. Ishikawa, M. Jakt, A. Kanapin, M. Katoh, Y. Kawasawa, J. Kelso, H. Kitamura, H. Kitano, G. Kollias, S. P. Krishnan, A. Kruger, S. K. Kummerfeld, I. V. Kurochkin, L. F. Lareau, D. Lazarevic, L. Lipovich, J. Liu, S. Liuni, S. McWilliam, M. Madan Babu, M. Madera, L. Marchionni, H. Matsuda, S. Matsuzawa, H. Miki, F. Mignone, S. Miyake, K. Morris, S. Mottagui-Tabar, N. Mulder, N. Nakano, H. Nakauchi, P. Ng, R. Nilsson, S. Nishiguchi, S. Nishikawa, F. Nori, O. Ohara, Y. Okazaki, V. Orlando, K. C. Pang, W. J. Pavan, G. Pavesi, G. Pesole, N. Petrovsky, S. Piazza, J. Reed, J. F. Reid, B. Z. Ring, M. Ringwald, B. Rost, Y. Ruan, S. L. Salzberg, A. Sandelin, C. Schneider, C. Schonbach, K. Sekiguchi, C. A. Semple, S. Seno, L. Sessa, Y. Sheng, Y. Shibata, H. Shimada, K. Shimada, D. Silva, B. Sinclair, S. Sperling, E. Stupka, K. Sugiura, R. Sultana, Y. Takenaka, K. Taki, K. Tammoja, S. L. Tan, S. Tang, M. S. Taylor, J. Tegner, S. A. Teichmann, H. R. Ueda, E. van Nimwegen, R. Verardo, C. L. Wei, K. Yagi, H. Yamanishi, E. Zabarovsky, S. Zhu, A. Zimmer, W. Hide, C. Bult, S. M. Grimmond, R. D. Teasdale, E. T. Liu, V. Brusic, J. Quackenbush, C. Wahlestedt, J. S. Mattick, D. A. Hume, C. Kai, D. Sasaki, Y. Tomaru, S. Fukuda, M. Kanamori-Katayama, M. Suzuki, J. Aoki, T. Arakawa, J. Iida, K. Imamura, M. Itoh, T. Kato, H. Kawaji, N. Kawagashira, T. Kawashima, M. Kojima, S. Kondo, H. Konno, K. Nakano, N. Ninomiya, T. Nishio, M. Okada, C. Plessy, K. Shibata, T. Shiraki, S. Suzuki, M. Tagami, K. Waki, A. Watahiki, Y. Okamura-Oho, H. Suzuki, J. Kawai, Y. Hayashizaki; FANTOM Consortium; RIKEN Genome Exploration Research Group and Genome Science Group (Genome Network Project Core Group), The transcriptional landscape of the mammalian genome. *Science* **309**, 1559–1563 (2005).
22. X. Cao, Z. Gao, C. E. Robert, S. Greene, G. Xu, W. Xu, E. Bell, D. Campbell, Y. Zhu, R. Young, M. Trucco, J. F. Markmann, A. Naji, B. A. Wolf, Pancreatic-derived factor (FAM3B), a novel islet cytokine, induces apoptosis of insulin-secreting beta-cells. *Diabetes* **52**, 2296–2303 (2003).
23. V. V. Pilipenko, A. Reece, D. I. Choo, J. H. Greinwald Jr., Genomic organization and expression analysis of the murine Fam3c gene. *Gene* **335**, 159–168 (2004).
24. H. Chen, X. Sun, W. Ge, Y. Qian, R. Bai, S. Zheng, A seven-gene signature predicts overall survival of patients with colorectal cancer. *Oncotarget* **8**, 95054–95065 (2017).
25. M. J. Pallen, B. W. Wren, The HtrA family of serine proteases. *Mol. Microbiol.* **26**, 209–221 (1997).
26. M. Horiba, K. Kadomatsu, K. Yasui, J. K. Lee, H. Takenaka, A. Sumida, K. Kamiya, S. Chen, S. Sakuma, T. Muramatsu, I. Kodama, Midkine plays a protective role against cardiac ischemia/reperfusion injury through a reduction of apoptotic reaction. *Circulation* **114**, 1713–1720 (2006).
27. B. Martin, G. Romero, G. Salama, Cardioprotective actions of relaxin. *Mol. Cell. Endocrinol.* **487**, 45–53 (2019).
28. T. Devarakonda, F. N. Salloum, Heart disease and relaxin: New actions for an old hormone. *Trends Endocrinol. Metab.* **29**, 338–348 (2018).
29. M. L. Lindsey, G. P. Escobar, R. Mukherjee, D. K. Goshorn, N. J. Sheats, J. A. Bruce, I. M. Mains, J. K. Hendrick, K. W. Hewett, R. G. Gourdie, L. M. Matrisian, F. G. Spinale, Matrix metalloproteinase-7 affects connexin-43 levels, electrical conduction, and survival after myocardial infarction. *Circulation* **113**, 2919–2928 (2006).
30. Y. A. Chiao, R. Zamilpa, E. F. Lopez, Q. Dai, G. P. Escobar, K. Hakala, S. T. Weintraub, M. L. Lindsey, In vivo matrix metalloproteinase-7 substrates identified in the left ventricle post-myocardial infarction using proteomics. *J. Proteome Res.* **9**, 2649–2657 (2010).
31. M. Shimano, N. Ouchi, K. Nakamura, Y. Oshima, A. Higuchi, D. R. Pimentel, K. D. Panse, E. Lara-Pezzi, S. J. Lee, F. Sam, K. Walsh, Cardiac myocyte-specific ablation of follistatin-like 3 attenuates stress-induced myocardial hypertrophy. *J. Biol. Chem.* **286**, 9840–9848 (2011).
32. E. Lara-Pezzi, L. E. Felkin, E. J. Birks, P. Sarathchandra, K. D. Panse, R. George, J. L. Hall, M. H. Yacoub, N. Rosenthal, P. J. Barton, Expression of follistatin-related genes is altered in heart failure. *Endocrinology* **149**, 5822–5827 (2008).
33. Y. Jiang, J. Bai, L. Tang, P. Zhang, J. Pu, Anti-CCL21 antibody attenuates infarct size and improves cardiac remodeling after myocardial infarction. *Cell. Physiol. Biochem.* **37**, 979–990 (2015).
34. A. Yndestad, A. V. Finsen, T. Ueland, C. Husberg, C. P. Dahl, E. Oie, L. E. Vinge, I. Sjaastad, O. Sandanger, T. Ranheim, K. Dickstein, J. Kjekshus, J. K. Damas, A. E. Fiane, D. Hilfiker-Kleiner, M. Lipp, L. Gullestad, G. Christensen, P. Aukrust, The homeostatic chemokine CCL21 predicts mortality and may play a pathogenic role in heart failure. *PLOS ONE* **7**, e33038 (2012).
35. J. T. Parissis, S. Adamopoulos, K. F. Venetsanou, D. G. Mentzikof, S. M. Karas, D. T. Kremastinos, Serum profiles of C-C chemokines in acute myocardial infarction: Possible implication in postinfarction left ventricular remodeling. *J. Interferon Cytokine Res.* **22**, 223–229 (2002).
36. S. C. de Jager, A. O. Kraaijeveld, R. W. Grauss, W. de Jager, S. S. Liem, B. L. van der Hoeven, B. J. Prakken, H. Putter, T. J. van Berkel, D. E. Atsma, M. J. Schalij, J. W. Jukema, E. A. Biessen, CCL3 (MIP-1 alpha) levels are elevated during acute coronary syndromes and show strong prognostic power for future ischemic events. *J. Mol. Cell. Cardiol.* **45**, 446–452 (2008).
37. D. Schumacher, S. Alampour-Rajabi, V. Ponomariov, A. Curaj, Z. Wu, M. Staudt, M. Rusu, V. Jankowski, N. Marx, J. Jankowski, V. Brandenburg, E. A. Liehn, A. Schuh, Cardiac FGF23: New insights into the role and function of FGF23 after acute myocardial infarction. *Cardiovasc. Pathol.* **40**, 47–54 (2019).
38. H. Hao, X. Li, Q. Li, H. Lin, Z. Chen, J. Xie, W. Xuan, W. Liao, J. Bin, X. Huang, M. Kitakaze, Y. Liao, FGF23 promotes myocardial fibrosis in mice through activation of β-catenin. *Oncotarget* **7**, 64649–64664 (2016).
39. S. Steffens, F. Montecucco, F. Mach, The inflammatory response as a target to reduce myocardial ischaemia and reperfusion injury. *Thromb. Haemost.* **102**, 240–247 (2009).
40. F. Montecucco, I. Bauer, V. Braunersreuther, S. Bruzzone, A. Akhmedov, T. F. Luscher, T. Speer, A. Poggi, E. Mannino, G. Pelli, K. Galan, M. Bertolotto, S. Lenglet, A. Garuti, C. Montessuit, R. Lerch, C. Pellieux, N. Vuilleumier, F. Dallegri, J. Mage, C. Sebastian, R. Mostoslavsky, A. Gayet-Ageron, F. Patrone, F. Mach, A. Nencioni, Inhibition of nicotinamide phosphoribosyltransferase reduces neutrophil-mediated injury in myocardial infarction. *Antioxid. Redox Signal.* **18**, 630–641 (2013).
41. C. Cappuzzello, L. Di Vito, R. Melchionna, G. Melillo, L. Silvestri, E. Cesareo, F. Crea, G. Liuzzo, A. Facchiano, M. C. Capogrossi, M. Napolitano, Increase of plasma IL-9 and decrease of plasma IL-5, IL-7, and IFN-γ in patients with chronic heart failure. *J. Transl. Med.* **9**, 28 (2011).
42. Y. Yang, C. Xu, S. Tang, Z. Xia, Interleukin-9 aggravates isoproterenol-induced heart failure by activating signal transducer and activator of transcription 3 signalling. *Can. J. Cardiol.* **36**, 1770–1781 (2020).
43. A. M. Marra, M. Arcopinto, A. Salzano, E. Bobbio, S. Milano, G. Misiano, F. Ferrara, O. Vriz, R. Napoli, V. Triggiani, P. Perrone-Filardi, F. Sacca, F. Giallauria, A. M. Isidori, C. Vigorito,

E. Bossone, A. Cittadini, Detectable interleukin-9 plasma levels are associated with impaired cardiopulmonary functional capacity and all-cause mortality in patients with chronic heart failure. *Int. J. Cardiol.* **209**, 114–117 (2016).
44. G. Bortolussi, L. Zentilin, G. Baj, P. Giraudi, C. Bellarosa, M. Giacca, C. Tiribelli, A. F. Muro, Rescue of bilirubin-induced neonatal lethality in a mouse model of Crigler-Najjar syndrome type I by AAV9-mediated gene transfer. *FASEB J.* **26**, 1052–1063 (2012).
45. F. Mingozzi, Y. L. Liu, E. Dobrzynski, A. Kaufhold, J. H. Liu, Y. Wang, V. R. Arruda, K. A. High, R. W. Herzog, Induction of immune tolerance to coagulation factor IX antigen by in vivo hepatic gene transfer. *J. Clin. Invest.* **111**, 1347–1356 (2003).
46. A. B. Gustafsson, R. A. Gottlieb, Autophagy in ischemic heart disease. *Circ. Res.* **104**, 150–158 (2009).
47. S. Kimura, T. Noda, T. Yoshimori, Dissection of the autophagosome maturation process by a novel reporter protein, tandem fluorescent-tagged LC3. *Autophagy* **3**, 452–460 (2007).
48. J. Hao, M. A. Daleo, C. K. Murphy, P. B. Yu, J. N. Ho, J. Hu, R. T. Peterson, A. K. Hatzopoulos, C. C. Hong, Dorsomorphin, a selective small molecule inhibitor of BMP signaling, promotes cardiomyogenesis in embryonic stem cells. *PLOS ONE* **3**, e2904 (2008).
49. M. Bujak, N. G. Frangogiannis, The role of TGF-beta signaling in myocardial infarction and cardiac remodeling. *Cardiovasc. Res.* **74**, 184–195 (2007).
50. S. Dennler, S. Itoh, D. Vivien, P. ten Dijke, S. Huet, J. M. Gauthier, Direct binding of Smad3 and Smad4 to critical TGF beta-inducible elements in the promoter of human plasminogen activator inhibitor-type 1 gene. *EMBO J.* **17**, 3091–3100 (1998).
51. J. F. Callahan, J. L. Burgess, J. A. Fornwald, L. M. Gaster, J. D. Harling, F. P. Harrington, J. Heer, C. Kwon, R. Lehr, A. Mathur, B. A. Olson, J. Weinstock, N. J. Laping, Identification of novel inhibitors of the transforming growth factor beta1 (TGF-beta1) type 1 receptor (ALK5). *J. Med. Chem.* **45**, 999–1001 (2002).
52. S. T. Magness, R. Bataller, L. Yang, D. A. Brenner, A dual reporter gene transgenic mouse demonstrates heterogeneity in hepatic fibrogenic cell populations. *Hepatology* **40**, 1151–1159 (2004).
53. C. Shih, R. A. Weinberg, Isolation of a transforming sequence from a human bladder carcinoma cell line. *Cell* **29**, 161–169 (1982).
54. Y. Feng, C. C. Broder, P. E. Kennedy, E. A. Berger, HIV-1 entry cofactor: Functional cDNA cloning of a seven-transmembrane, G protein-coupled receptor. *Science* **272**, 872–877 (1996).
55. K. Takahashi, S. Yamanaka, Induction of pluripotent stem cells from mouse embryonic and adult fibroblast cultures by defined factors. *Cell* **126**, 663–676 (2006).
56. S. Zacchigna, L. Zentilin, M. Giacca, Adeno-associated virus vectors as therapeutic and investigational tools in the cardiovascular system. *Circ. Res.* **114**, 1827–1846 (2014).
57. P. Garcia-Olloqui, J. R. Rodriguez-Madoz, M. Di Scala, G. Abizanda, A. Vales, C. Olague, O. Iglesias-Garcia, E. Larequi, L. P. Aguado-Alvaro, A. Ruiz-Villalba, F. Prosper, G. Gonzalez-Aseguinolaza, B. Pelacho, Effect of heart ischemia and administration route on biodistribution and transduction efficiency of AAV9 vectors. *J. Tissue Eng. Regen. Med.* **14**, 123–134 (2020).
58. J. Abadie, V. Blouin, L. Guigand, M. Wyers, Y. Cherel, Recombinant adeno-associated virus type 2 mediates highly efficient gene transfer in regenerating rat skeletal muscle. *Gene Ther.* **9**, 1037–1043 (2002).
59. A. Sumida, M. Horiba, H. Ishiguro, H. Takenaka, N. Ueda, H. Ooboshi, T. Opthof, K. Kadomatsu, I. Kodama, Midkine gene transfer after myocardial infarction in rats prevents remodelling and ameliorates cardiac dysfunction. *Cardiovasc. Res.* **86**, 113–121 (2010).
60. S. Fukui, S. Kitagawa-Sakakida, S. Kawamata, G. Matsumiya, N. Kawaguchi, N. Matsuura, Y. Sawa, Therapeutic effect of midkine on cardiac remodeling in infarcted rat hearts. *Ann. Thorac. Surg.* **85**, 562–570 (2008).
61. K. L. Christman, Q. Fang, M. S. Yee, K. R. Johnson, R. E. Sievers, R. J. Lee, Enhanced neovasculature formation in ischemic myocardium following delivery of pleiotrophin plasmid in a biopolymer. *Biomaterials* **26**, 1139–1144 (2005).
62. B. Sun, R. Huo, Y. Sheng, Y. Li, X. Xie, C. Chen, H. B. Liu, N. Li, C. B. Li, W. T. Guo, J. X. Zhu, B. F. Yang, D. L. Dong, Bone morphogenetic protein-4 mediates cardiac hypertrophy, apoptosis, and fibrosis in experimentally pathological cardiac hypertrophy. *Hypertension* **61**, 352–360 (2013).
63. Y. Zhu, G. Xu, A. Patel, M. M. McLaughlin, C. Silverman, K. Knecht, S. Sweitzer, X. Li, P. McDonnell, R. Mirabile, D. Zimmerman, R. Boyce, L. A. Tierney, E. Hu, G. P. Livi, B. Wolf, S. S. Abdel-Meguid, G. D. Rose, R. Aurora, P. Hensley, M. Briggs, P. R. Young, Cloning, expression, and initial characterization of a novel cytokine-like gene family. *Genomics* **80**, 144–150 (2002).
64. P. Johansson, J. Bernstrom, T. Gorman, L. Oster, S. Backstrom, F. Schweikart, B. Xu, Y. Xue, L. H. Schiavone, FAM3B PANDER and FAM3C ILEI represent a distinct class of signaling molecules with a non-cytokine-like fold. *Structure* **21**, 306–313 (2013).
65. C. E. Robert-Cooperman, J. R. Carnegie, C. G. Wilson, J. Yang, J. R. Cook, J. Wu, R. A. Young, B. A. Wolf, B. R. Burkhardt, Targeted disruption of pancreatic-derived factor (PANDER, FAM3B) impairs pancreatic beta-cell function. *Diabetes* **59**, 2209–2218 (2010).
66. J. Yang, C. E. Robert, B. R. Burkhardt, R. A. Young, J. Wu, Z. Gao, B. A. Wolf, Mechanisms of glucose-induced secretion of pancreatic-derived factor (PANDER or FAM3B) in pancreatic beta-cells. *Diabetes* **54**, 3217–3228 (2005).
67. A. Bendre, K. G. Buki, J. A. Maatta, Fam3c modulates osteogenic differentiation by down-regulating Runx2. *Differentiation* **93**, 50–57 (2017).
68. T. Waerner, M. Alacakaptan, I. Tamir, R. Oberauer, A. Gal, T. Brabletz, M. Schreiber, M. Jechlinger, H. Beug, ILEI: A cytokine essential for EMT, tumor formation, and late events in metastasis in epithelial cells. *Cancer Cell* **10**, 227–239 (2006).
69. Z. Chen, L. Ding, W. Yang, J. Wang, L. Chen, Y. Chang, B. Geng, Q. Cui, Y. Guan, J. Yang, Hepatic activation of the FAM3C-HSF1-CaM pathway attenuates hyperglycemia of obese diabetic mice. *Diabetes* **66**, 1185–1197 (2017).
70. S. Sciarretta, Y. Maejima, D. Zablocki, J. Sadoshima, The Role of Autophagy in the Heart. *Annu. Rev. Physiol.* **80**, 1–26 (2018).
71. L. A. Kirshenbaum, Regulation of autophagy in the heart in health and disease. *J. Cardiovasc. Pharmacol.* **60**, 109 (2012).
72. M. Taneike, O. Yamaguchi, A. Nakai, S. Hikoso, T. Takeda, I. Mizote, T. Oka, T. Tamai, J. Oyabu, T. Murakawa, K. Nishida, T. Shimizu, M. Hori, I. Komuro, T. S. Takuji Shirasawa, N. Mizushima, K. Otsu, Inhibition of autophagy in the heart induces age-related cardiomyopathy. *Autophagy* **6**, 600–606 (2010).
73. L. M. D. Delbridge, K. M. Mellor, D. J. Taylor, R. A. Gottlieb, Myocardial stress and autophagy: Mechanisms and potential therapies. *Nat. Rev. Cardiol.* **14**, 412–425 (2017).
74. A. Desmouliere, A. Geinoz, F. Gabbiani, G. Gabbiani, Transforming growth factor-beta 1 induces alpha-smooth muscle actin expression in granulation tissue myofibroblasts and in quiescent and growing cultured fibroblasts. *J. Cell Biol.* **122**, 103–111 (1993).
75. P. J. Sime, Z. Xing, F. L. Graham, K. G. Csaky, J. Gauldie, Adenovector-mediated gene transfer of active transforming growth factor-beta1 induces prolonged severe fibrosis in rat lung. *J. Clin. Invest.* **100**, 768–776 (1997).
76. J. Zumbrunn, B. Trueb, Primary structure of a putative serine protease specific for IGF-binding proteins. *FEBS Lett.* **398**, 187–192 (1996).
77. S. Launay, E. Maubert, N. Lebeurrier, A. Tennstaedt, M. Campioni, F. Docagne, C. Gabriel, L. Dauphinot, M. C. Potier, M. Ehrmann, A. Baldi, D. Vivien, HtrA1-dependent proteolysis of TGF-beta controls both neuronal maturation and developmental survival. *Cell Death Differ.* **15**, 1408–1416 (2008).
78. A. Csiszar, B. Kutay, S. Wirth, U. Schmidt, S. Macho-Maschler, M. Schreiber, M. Alacakaptan, G. F. Vogel, K. Aumayr, L. A. Huber, H. Beug, Interleukin-like epithelial-to-mesenchymal transition inducer activity is controlled by proteolytic processing and plasminogen-urokinase plasminogen activator receptor system-regulated secretion during breast cancer progression. *Breast Cancer Res.* **16**, 433 (2014).
79. M. Kral, C. Klimek, B. Kutay, G. Timelthaler, T. Lendl, B. Neuditschko, C. Gerner, M. Sibilia, A. Csiszar, Covalent dimerization of interleukin-like epithelial-to-mesenchymal transition (EMT) inducer (ILEI) facilitates EMT, invasion, and late aspects of metastasis. *FEBS J.* **284**, 3484–3505 (2017).

Acknowledgments: We are grateful to P. Confalonieri, F. Vacante, C. Radesich, M. Sansonetti, F. Loffredo, L. Camparini, R. Noè, and R. Artioli for support in some of the experiments.
Funding: This work was supported by the British Heart Foundation (BHF) Programme Grant RG/19/11/34633, the European Research Council (ERC) Advanced Grant 787971 "CuRE", the King's College London BHF Centre of Research Excellence grant RE/18/2/34213, and grants 825670 "CardioReGenix" and 874764 "REANIMA" from the European Commission Horizon 2020 programme, along with the continuous support of Fondazione CRTrieste, Trieste, Italy. **Author contributions:** G.R. and F.B. generated the AAV library, performed sequencing and bioinformatic analysis, and conducted or coordinated factor characterization. A.F. and V.M. provided technical support. A.M. and L.B. contributed to factor characterization. S.V., M.T., M.D.F., and S.Z. performed the animal experiments. A.C. analyzed the echocardiography data. L.Z. produced AAV vectors. G.S. provided clinical advice. M.G. conceived and coordinated the study. All the authors had access to the data and contributed to their analysis. **Competing interests:** M.G., G.R., and F.B. are inventors on a patent application (U.K. no. 1906052.4) submitted by ICGEB that covers the use of Chrdl1, Fam3c, and Fam3b as cardioprotective factors. This patent is assigned to Forcefield Therapeutics, London, for which M.G. is a founder, member of the board, equity holder, and consultant, and F.B. is a consultant. The AAV secretome library and the FunSel technology are owned by Purespring Therapeutics, for which M.G. is a cofounder, observer to the board, equity holder, and consultant. **Data and materials availability:** All data associated with this study are present in the paper or the Supplementary Materials. Plasmid vectors and other constructs are available from the Molecular Medicine Laboratory of ICGEB under a material transfer agreement with ICGEB.

Submitted 12 January 2022
Accepted 10 August 2022
Published 31 August 2022
10.1126/scitranslmed.abo0699